**Article:**
Ghalambaz, M, Tahmasebi, A, Chamkha, AJ et al. (2019) Conjugate local thermal non-equilibrium heat transfer in a cavity filled with a porous medium: Analysis of the element location. International Journal of Heat and Mass Transfer, 138. pp. 941-960. ISSN: 0017-9310

https://doi.org/10.1016/j.ijheatmasstransfer.2019.03.073

# Conjugate local thermal non-equilibrium heat transfer in a cavity filled with a porous medium: Analysis of the element location

**M. Ghalambaz[1,2], A. Tahmasbi[3], and A. J. Chamkha[3,4] D. Wen[1,5]**

[1]School of Aeronautic Science and Engineering, Beihang University, Beijing, P.R.China

[2]Department of Mechanical Engineering, Dezful Branch, Islamic Azad University, Dezful, Iran

[3]Shahid Chamran University of Ahvaz, Ahvaz, Iran.

[4]Mechanical Engineering Department, Prince Sultan Endowment for Energy and Environment, Prince Mohammad Bin Fahd University, Al-Khobar 31952, Saudi Arabia

[5]RAK Research and Innovation Center, American University of Ras Al Khaimah, United Arab Emirates

[5]School of Chemical and Process Engineering, University of Leeds, Leeds, U,K

## Abstract

The problem of conjugate natural convection heat transfer in a cavity filled with a porous medium is addressed by considering the local thermal non-equilibrium effects. The thickness of the solid walls of the cavity is taken into account, and the vertical walls are assumed to be partially active. The effect of the heat transfer bifurcation in the interface of the solid walls and the porous medium is also taken into account. The governing equations for the heat and momentum of the fluid in the porous space, heat transfer in the porous matrix, and heat transfer in the solid walls are represented in the form of partial differential equations. The governing equations along with the corresponding boundary conditions are transformed to a generalized form of the non-dimensional equations, and solved by the finite element method . Considering various values of the non-dimensional parameters, the effect of the location of the active walls

on the flow patterns and the local and overall heat transfer are addressed. The results demonstrate that the location of the active walls can significantly affect the streamlines and the fluid isotherm contours in the porous space and the isotherms in the solid walls. Moreover, it is found that in most of the cases the highest total rate of heat transfer corresponds to the case in which the elements are in the centre of the active wells. In contrast, the lowest total rate of the heat transfer corresponds to a case, in which the active hot element is at the top of the wall and the cold element is at the bottom.

**Nomenclature**

Latin Symbols

| | |
|---|---|
| *al, ar* | length of left and right thermally active locations, respectively (m) |
| *Al, Ar* | dimensionless length of left and right thermally active locations, respectively |
| *d* | wall thickness (m) |
| *D* | wall thickness to height ratio |
| *Da* | Darcy number |
| g | gravitational acceleration vector (m $s^{-2}$) |
| $h_{fs}$ | volumetric heat transfer coefficient between the fluid and solid (W $m^{-3}$ $K^{-1}$) |
| *H* | porous-fluid interface convection parameter |
| *k* | thermal conductivity (W $m^{-1}$ $K^{-1}$) |
| *K* | permeability of the porous medium ($m^2$) |

| | |
|---|---|
| $K_r$ | porous-fluid thermal conductivity ratio parameter |
| $L$ | square cavity wall length (m) |
| $M$ | mesh size parameter |
| $Nu$ | average Nusselt number |
| $Nu_y$ | local Nusselt number in the porous and in the free fluid |
| $p$ | Pressure in the porous and free fluid (Pa) |
| $P$ | dimensionless pressure |
| $Pr$ | Prandtl number of the fluid |
| $q''$ | heat flux (W $m^{-2}$) |
| $Q_w$ | dimensionless average heat transfer through the walls |
| $Q_{w,y}$ | dimensionless heat transfer through the walls |
| $Ra$ | Rayleigh number |
| $R_k$ | wall to fluid thermal conductivity ratio parameter |
| $T$ | temperature (K) |
| $u$, $v$ | velocity components along $x$, $y$ directions, respectively (m $s^{-1}$) |
| $U$, $V$ | dimensionless velocity components along $x$, $y$ directions, respectively |
| $x$, $y$ | Cartesian coordinates (m) |
| $X$, $Y$ | dimensionless Cartesian coordinates |

*ypl, ypr* position of left and right thermally active locations, respectively (m)

*Ypl, Ypr* dimensionless position of left and right thermally active locations, respectively

Greek symbols

$\alpha$ effective thermal diffusivity ($m^2\ s^{-1}$)

$\beta$ thermal expansion coefficient of the fluid ($K^{-1}$)

$\Delta$ difference value

$\varepsilon$ porosity of the porous medium

$\theta$ dimensionless temperature

$\mu$ dynamic viscosity ($kg\ m^{-1}\ s^{-1}$)

$\nu$ kinematic viscosity ($m^2\ s^{-1}$)

$\rho$ density ($kg\ m^{-3}$)

$(\rho c)$ effective heat capacity ($J\ K^{-1}\ m^{-3}$)

$\varphi$ angle of inclination of side walls represented in Table 1 (degree)

$\Psi$ dimensionless stream function

Subscripts

0 ambient property

*c* cold

*eff* effective

| | |
|---|---|
| *f* | fluid |
| *h* | hot |
| max | maximum |
| *s* | solid |
| *t* | total |
| *w* | wall |

## 1. Introduction

The convective heat transfer in a cavity filled with a porous medium is an important subject in many engineering applications, including geothermal systems, insulation systems, heat exchangers, fuel cells, chemical reactors and solar thermal systems. For example, the metal foams [1] and porous media heat sinks [2] have been utilized for dissipating the generated heat in the electronic devices into atmosphere. As proposed in [3] a thermally conductive porous media can be linked to a heat spreading interfacial material to dissipate heat from a heat source.

As another example of convective heat transfer in a cavity filled with a porous medium, a cooling jacket involves a thermal conductive porous matrix in which the main body of the jacket is sandwiched between two conductive plates, and there is a liquid in the porous matrix, which can flow in the porous space between the plates. Indeed, the plates are thermal interfaces, which connect a high temperature device or system to the atmosphere or other parts of the system. A cooling jacket can protect the high temperature devices from temperature overload damage. A simple cooling jacket can be seen as a cavity filled with a porous medium subjecting to conjugate heat transfer in the cooling jacket walls. Recently, the thermal conductive metal foams have been employed to enhance the heat transfer in heat exchangers [4]. There are one

or more passages in a heat exchanger, in which some of the passages can be supported by a metal foam. The metal foam can provide a desirable balance of heat exchange properties within the passages and the fluid in the heat exchanger [4].

In a case in which the convective heat transfer between the fluid and solid matrix of the porous medium is high or in a case in which the thermal conductivity of the porous matrix is very low, the temperature of the fluid and the porous matrix can be assumed to be identical. In these cases, the local thermal equilibrium approach may ~~be~~ adequately model the heat transfer in porous media.

With regard to the local thermal equilibrium model, Basak et al. [5] and Sathiyamoorthy et al. [6] have studied the effect of imposing a non-uniform thermal boundary condition on the natural convection heat transfer in an enclosure filled with a saturated porous medium. These researchers have analysed the effect of imposing a sinusoidally-shaped temperature variation at the bottom wall [5] and side walls [6] of the cavity. Sheremet and Pop [7] extended the study of Sathiyamoorthy et al. [6] to the case of nanofluids. Varol et al. [8] investigated the effect of the shape of the cavity and the inclination angle on the heat and fluid characteristics of natural convection in a cavity filled with a porous medium. Chamkha and Ismael [9] addressed the natural convective heat transfer in a differentially difference heated cavity partially filled with a porous medium. Sheremet et al. [10] analyzed the convective heat transfer of nanofluids in a differentially difference heated cavity. Saeid and Pop [11] addressed the natural convection heat transfer in a cavity filled with a Darcy porous medium. The cavity in [11] was differentially heated from side walls and well insulated at the top and bottom walls. The entire of the cold vertical wall was subjected to cold temperature of $T_c$, while the hot wall was partially heated by an element providing a constant hot temperature or heat flux. The rest of the hot vertical wall was left insulated.

These researchers [11] have studied the effect of the length and the position of the element on the temperature patterns and the average Nusselt number in the cavity for the Darcy-Rayleigh number in the range of 10-1000. The results showed that the location of the heater for obtaining the maximum average Nusselt number was a function of Rayleigh-Darcy number. For a case with high Rayleigh-Darcy number, the maximum average Nusselt number occurred for an element located next to the bottom of the cavity. However, as the Rayleigh-Darcy number decreased, the location of the element for maximum average Nusselt number shifts upward. Saeid and Pop [12] have also studied the un-steady natural convection in a differentially heated side walls cavity filled with a porous medium. They applied a step temperature difference to the side walls by suddenly cooling one wall and heating another one. The results showed that during the transient period, the average Nusselt number at the walls went through undershoot and then reached ~~to~~ its steady state value. The transient time was a function of the Darcy-Rayleigh number in a way that the increase of the Rayleigh number decreased the transient period. Sheremet et al. [13, 14] have considered the unsteady heat transfer of nanofluids in cavities.

Considering the local thermal equilibrium approach and the conjugate heat transfer, Baytaş et al. [15] studied the natural convective heat transfer in a differentially heated square cavity filled with a porous medium. The side walls of the cavity were imposed to a temperature difference and the top and bottom walls are insulated. There was a layer of thick thermal conductive solid wall over the bottom and top horizontal walls. The effect of wall thermal conductivity on the heat transfer was addressed. The results revealed that the coupling effect with the conductive wall (conjugate heat transfer) was only important for the cases with high thermal conductive walls. Hence, it was concluded that a high thermal conductive wall can significantly alter the heat and flow characteristics in the cavity. Saeid [16, 17] studied the conjugate natural convection heat transfer in a cavity with differentially heated side walls filled

with a porous medium while there wss a layer of solid wall one [16] or two side walls [17]. Following the study of Saied [17], Alhashash et al. [18] considered the radiation and heat generation effects while Sheremet and Pop [19] investigated the natural convection heat transfer of nanofluids. Saleh et al. [20] and Ismael et al. [21] analysed the conjugate natural convection heat transfer in a square cavity induced by a thick hot solid plate mounted at the bottom of the cavity.

There are various cases in which assuming a local thermal equilibrium between the fluid and porous matrix is not adequate. For example, when the porous matrix is highly thermal conductive or when the interface convective heat transfer between the fluid and the porous matrix is very low, the temperature difference between the fluid and the porous matrix could be significant. The heat sinks or metal foam in the atmospheric conditions with low fluid motions are common engineering applications in this case. Another example is when there is a significance internal heat generation either in the fluid or porous matrix phase. For instance, the nuclear fuel rods in the reactor pool, filled with water, is an engineering example of this type of application, in which the heat generation occurs in the solid phase. When the temperature difference between the fluid and porous matrix is significant, it is essential to utilize the Local Thermal Non-Equilibrium (LTNE) approaches.

When considering the local thermal non-equilibrium approach, Baytas and Pop [22] and Baytas [23] addressed the natural convection heat transfer in an enclosure cavity filled with a saturated porous medium. Wu et al. [24] investigated the effect of non-uniform sinusoidally shape wall temperature on the natural convection in a square cavity. The authors revealed that the overall heat transfer (Nusselt number) can be improved by imposing sinusoidal thermal boundary condition when compared to the case of a constant wall temperature. Wu et al. [25] also analysed the effect non uniform wall temperature on the natural convection heat transfer in a cavity by considering a linear variation of the wall temperature. Other aspects of LTNE

natural convection in a cavity, such as the effects of partially active wall with sinusoidal temperature [25], cavity aspect ratio [26], nanofluids [27] and cavity partially filled with porous media [28], have been addressed in the literature.

When considering LTNE, Yang and Vafai [29-31] ~~have~~ discussed the possible heat transfer boundary conditions at the interface of porous media, fluid and walls. Furthermore, an excellence discussion about the possible boundary conditions for heat coupling at the wall interface of porous media and fluid can be found in the studies of Nield [32] and Vafai and Yang [33].

A review of the literature ~~by~~ considering LTNE conjugate natural convection shows that the studies that have addressed conjugate LTNE in cavities are very limited . Saeid [34] has analysed LTNE conjugate natural convection heat transfer in a square cavity. In the study of Saeid [34], the vertical cavity side walls were subject to a temperature difference, while the top and bottom walls are well insulated. A future literature review shows that despite the very important engineering application of LTNE conjugate natural convection heat transfer in porous media, this phenomenon has been extensively overlooked in previous studies.

Following the study of Saeid [34], the present study aims to address the effect of the location of the heating element on the flow and heat transfer characteristics of natural convection in a cavity filled with a porous medium using the LTNE approach.

The present study aims to answer the following fundamental questions:

1- What is the effect of the location of the hot and cold elements on the active walls?

2- Is there an optimum location for the placement of the elements to reach the lowest or the highest total heat transfer rate in the cavity?

3- Does the thickness and the thermal conductivity of the active walls affect the thermal behaviour of the cavity and the important locations of the active elements?

4- How does the LTNE effect alter the thermal behaviour of the cavity?

## 2. Mathematical model and governing equations

Fig. 1 shows the schematic view of the physical model of the present study. As seen, there is a cavity with the size $L$ in which a layer of porous medium is sandwiched between two vertical thick walls of thickness $d$. The porous medium is homogeneous with the porosity of $\varepsilon$ and permeability of $K$ which is saturated by a Newtonian fluid. The top and bottom walls of the cavity are well insulated. A flash element with the constant temperature of $T_h$ and the length of $al$ is mounted at the location of $ypl$ at the vertical left wall while the rest of the wall is well insulated. The right wall is imposed to a radiator with the constant temperature of $T_c$, the length $ar$ and the centre of location of $ypr$ while the rest of the wall is well insulated. The thick walls are thermal conductive with the thermal conductivity coefficient of $k$.

An overall view of the physic of the heat transfer in the cavity shows that heat tends to diffuse in the solid wall until it reaches ~~to~~ the wall interface with the porous medium. In the interface of the porous, there is an energy balance between the heat which reaches the wall surface from the element and the heat which transfers to the porous matrix and the fluid. Indeed, there are two channels for heat transfer in the porous matrix, one through the porous matrix and the other one through the fluid. Therefore, when the heat from the element reaches ~~to~~ the wall interface, a portion of the heat tends to diffuse in the porous matrix and the rest of the heat tends diffuse in the fluid.

It can be concluded that at the wall interface the thermal energy of the solid wall, the fluid and the porous matrix are coupled. As the fluid next to the wall interface gets hot, the density of the fluid decreases, and hence it tends to move upward and form a natural convection regime in the porous medium. By increasing the buoyancy forces (due to the temperature gradient in the fluid) the motion of the fluid gets stronger, and consequently the heat transfer due to fluid motion boosts. The heat in the porous layer goes in complex directions. In fact, it

can diffuse in the fluid as it moves with the fluid flow. It can move into or out of the porous matrix as there is a temperature difference between the fluid and the porous matrix, and it can also diffuse in the porous matrix as the porous matrix is thermal conductive. Finally, the heat reaches ~~to~~ the wall interface of the solid wall with the radiator. As the diffusion in the wall and the coupling of the heat at the wall interface are two important paths of heat transfer in the cavity, the location of the flash element and radiator could induce a significant effect upon the flow and heat characteristics in the cavity. Thus, considering the location of the flash element and the radiator, nine main configurations for these elements that can be assumed are depicted in Fig. 2. These configurations and their effects on the flow and heat transfer in the cavity will be examined in this study.

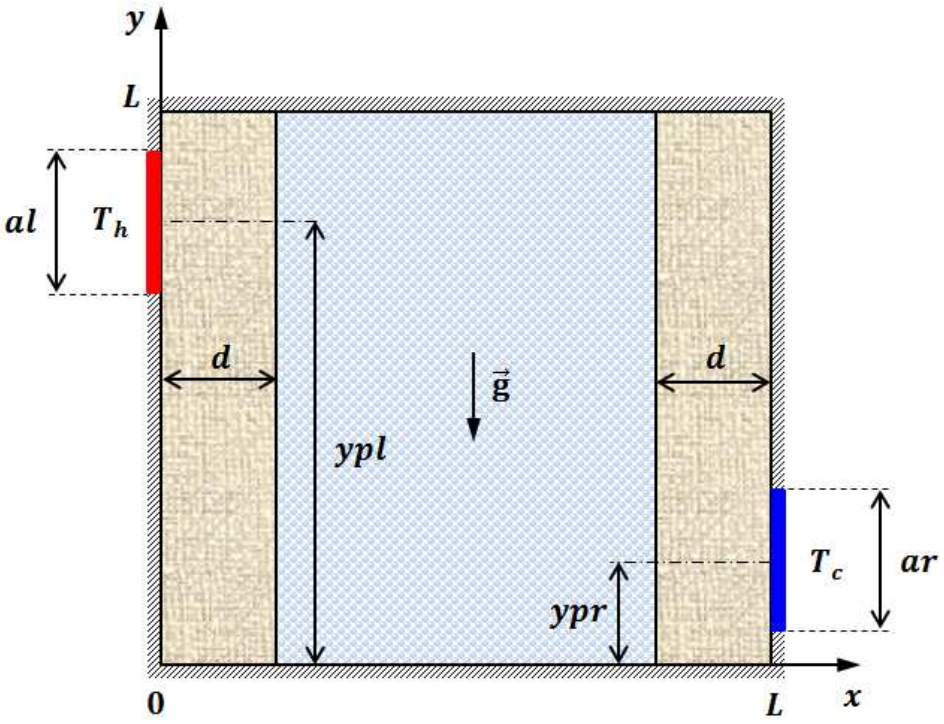


**Fig. 1.** Schematic view of the coordinate system and the physical model.

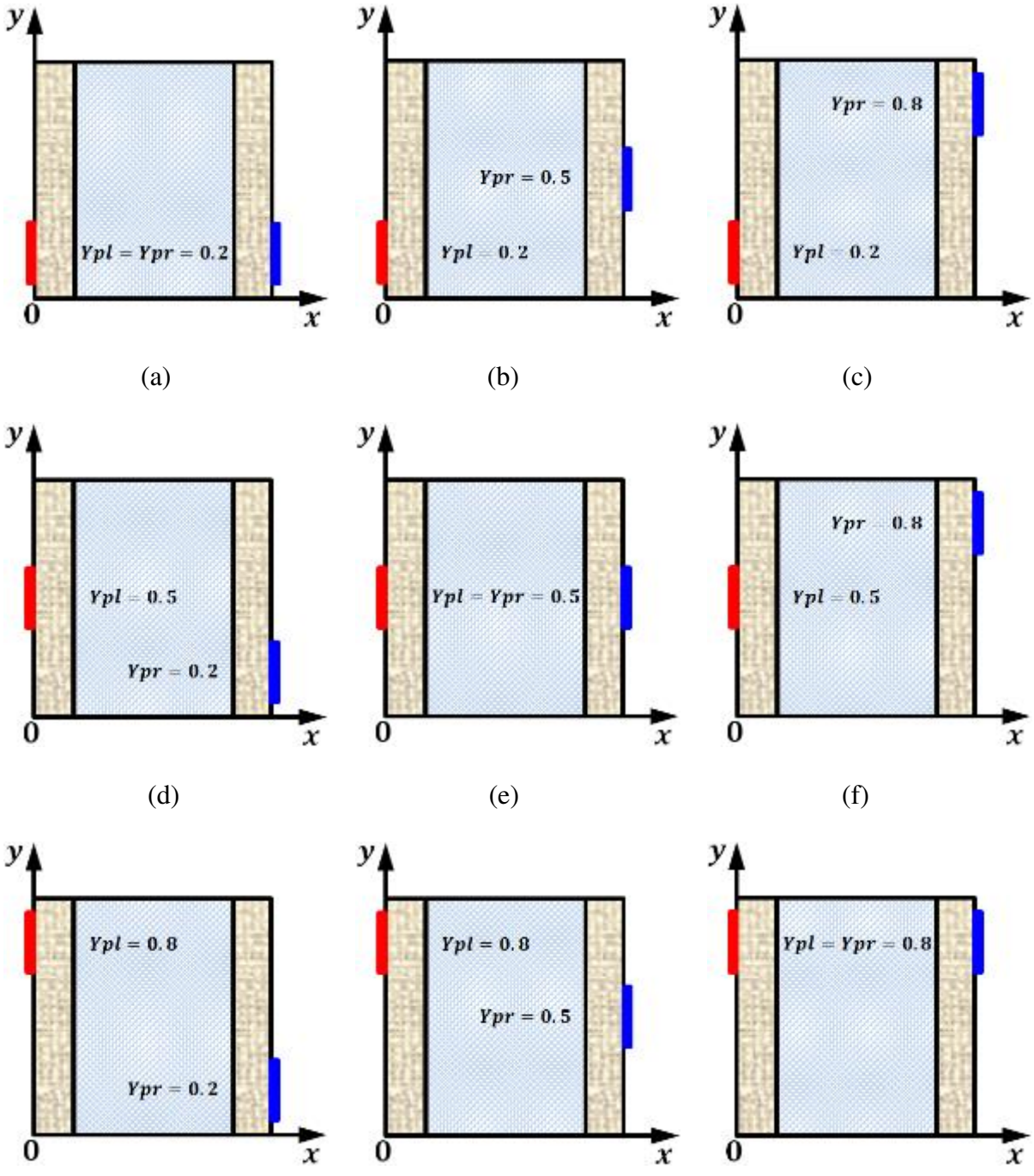


**Fig. 2.** Different cases of thermally active Locations.

In the modelling of local thermal non-equilibrium conjugate heat transfer in the cavity, the following assumptions are adopted: the temperature difference in the cavity is not high and hence the thermophysical properties for the fluid, porous matrix and the solid wall can be assumed as constant except the variation which causes the buoyancy forces in the momentum

equation. The buoyancy forces are incorporated in the momentum equation using the Oberbeck-Boussinesq approximation. In the porous medium, the extended Darcy-Brinkman model is utilized to model the fluid motion and its interaction with the porous medium. Two energy conversion equations, one for fluid and one for porous matrix, are adopted. The energy equations are coupled using the porous-fluid interface equations. With these assumptions, the continuity, momentum, and energy equations for the steady, two-dimensional flow in an isotropic and homogeneous porous medium can be written as [35-38]:

$$\frac{\partial u}{\partial x}+\frac{\partial v}{\partial y}=0 \tag{1}$$

$$\frac{\rho_f}{\varepsilon^2}\left(u\frac{\partial u}{\partial x}+v\frac{\partial u}{\partial y}\right)=-\frac{\partial p}{\partial x}+\frac{\mu_f}{\varepsilon}\left(\frac{\partial^2 u}{\partial x^2}+\frac{\partial^2 u}{\partial y^2}\right)-\frac{\mu_f}{K}u \tag{2}$$

$$\frac{\rho_f}{\varepsilon^2}\left(u\frac{\partial v}{\partial x}+v\frac{\partial v}{\partial y}\right)=-\frac{\partial p}{\partial y}+\frac{\mu_f}{\varepsilon}\left(\frac{\partial^2 v}{\partial x^2}+\frac{\partial^2 v}{\partial y^2}\right)-\frac{\mu_f}{K}v+\rho_f\beta\left(T_f-T_c\right)g \tag{3}$$

$$\frac{1}{\varepsilon}\left(u\frac{\partial T_f}{\partial x}+v\frac{\partial T_f}{\partial y}\right)=\alpha_f\left(\frac{\partial^2 T_f}{\partial x^2}+\frac{\partial^2 T_f}{\partial y^2}\right)+\frac{h_{fs}\left(T_s-T_f\right)}{\varepsilon\left(\rho c\right)_f} \tag{4}$$

$$0=\alpha_s\left(\frac{\partial^2 T_s}{\partial x^2}+\frac{\partial^2 T_s}{\partial y^2}\right)+\frac{h_{fs}}{\left(1-\varepsilon\right)\left(\rho c\right)_s}\left(T_f-T_s\right) \tag{5}$$

where $u$ and $v$ are Darcy velocities in the $x$ and $y$ directions respectively. Here, $p$ and $T_f$ denote the pressure and the temperature of the fluid, $T_s$ denotes the porous matrix temperature. $\rho_f$, $\mu_f$, $\alpha_f$, and $c_f$ denote the density, the dynamic viscosity, the thermal diffusivity and the specific heat capacity of the fluid, respectively. It is worth noticing that the utilization of effective dynamic viscosity in porous media is common, which is written as $\mu_{eff} = \mu_f / \varepsilon$. The thermal diffusivity of the fluid, $\alpha_f$ is introduced as $k_f/(\rho_f c_f)$ where $k_f$ is the thermal conductivity of the fluid. In the $y$-momentum equation, Eq. (3), the term $\rho_f\beta\,(T_f - T_c)\,g$ shows the body force due to the buoyancy

forces, and couples the fluid momentum equation with the energy equation of the fluid. In the term of the buoyancy forces, $\beta$ is the fluid thermal volume expansion coefficient and $g$ is the gravitational constant. In the energy equations, Eqs. (4) and (5), the terms involving $h_{fs}$ are the porous-fluid interface heat transfer terms which couples the heat transfer between the porous medium and the fluid in the domain of the porous layer; $h_{fs}$ is the convective heat transfer coefficient between the porous medium and fluid. The energy equation in each of the solid walls can be written as

$$k_w\left(\frac{\partial^2 T_w}{\partial x^2}+\frac{\partial^2 T_w}{\partial y^2}\right)=0 \tag{6}$$

where $T_w$ indicates the temperature of the solid wall, and $k_w$ indicates the thermal conductivity of the solid wall.

The momentum boundary conditions are considered as zero velocities ($u$=$v$=0) at the wall interfaces. A reference pressure of $p$ ($d$, $L$) = 0 is also considered at the top corner of the porous layer. Moreover, the following boundary conditions are considered for the energy equations. The thermal boundary conditions at the flush element and the radiator are $T_w$=$T_h$ and $T_w$=$T_c$, respectively. The insulation at the top and bottom walls is employed as $\partial T/\partial y=0$ where $T$=$T_f$, $T_s$ and $T_w$. The thermal boundary condition at the walls interfaces is the energy balance which, using the Fourier's law, can be written as $k_w\frac{\partial T_w}{\partial x}=\varepsilon k_f\frac{\partial T_f}{\partial x}+\left(1-\varepsilon\right)k_s\frac{\partial T_s}{\partial x}$ on $x=d$, $x=1-d$, $0\le y\le 1$. Here, $\varepsilon\times k_f$ and $(1\text{-}\varepsilon)\times k_s$ represent the effective thermal conductivity of the fluid and the effective thermal conductivity of the porous matrix at the wall interface. Now, in order to generalize the study, the non-dimensional variables in the following form are introduced

$$
\begin{aligned}
&X = \frac{x}{L},\ Y = \frac{y}{L},\ D = \frac{d}{L},\ Ypl = \frac{ypl}{L},\ Ypr = \frac{ypr}{L},\\
&Al = \frac{al}{L}, Ar = \frac{ar}{L}, Pr = \frac{\upsilon_f}{\alpha_f},\ U = \frac{uL}{\alpha_f},\ V = \frac{vL}{\alpha_f}, P = \frac{pL^2}{\rho_f \alpha_f{}^2},\\
&\theta_f = (T_f - T_c)/(T_h - T_c),\ \theta_s = (T_s - T_c)/(T_h - T_c),\ \theta_w = (T_w - T_c)/(T_h - T_c)
\end{aligned}
\tag{7}
$$

and utilized to transform the governing equations into a non-dimensional form. Invoking the non-dimensional parameters and variables introduced in Eq. (7), the following non-dimensional form of governing Eqs. (1)-(6) is obtained:

$$\frac{\partial U}{\partial X} + \frac{\partial V}{\partial Y} = 0 \tag{8}$$

$$\frac{1}{\varepsilon^2}\left(U\frac{\partial U}{\partial X} + V\frac{\partial U}{\partial Y}\right) = -\frac{\partial P}{\partial X} + \frac{Pr}{\varepsilon}\left(\frac{\partial^2 U}{\partial X^2} + \frac{\partial^2 U}{\partial Y^2}\right) - \frac{Pr}{Da}U \tag{9}$$

$$\frac{1}{\varepsilon^2}\left(U\frac{\partial V}{\partial X} + V\frac{\partial V}{\partial Y}\right) = -\frac{\partial P}{\partial Y} + \frac{Pr}{\varepsilon}\left(\frac{\partial^2 V}{\partial X^2} + \frac{\partial^2 V}{\partial Y^2}\right) - \frac{Pr}{Da}V + Ra \cdot Pr \cdot \theta_f \tag{10}$$

$$\frac{1}{\varepsilon}\left(U\frac{\partial \theta_f}{\partial X} + V\frac{\partial \theta_f}{\partial Y}\right) = \frac{\partial^2 \theta_f}{\partial X^2} + \frac{\partial^2 \theta_f}{\partial Y^2} + H\left(\theta_s - \theta_f\right) \tag{11}$$

$$0 = \frac{\partial^2 \theta_s}{\partial X^2} + \frac{\partial^2 \theta_s}{\partial Y^2} + H \cdot K_r\left(\theta_f - \theta_s\right) \tag{12}$$

$$\frac{\partial^2 \theta_w}{\partial X^2} + \frac{\partial^2 \theta_w}{\partial Y^2} = 0 \tag{13}$$

where *Da* is the Darcy number, *Ra* is the Rayleigh number, *H* is the porous-fluid interface convection parameter and $K_r$ is the porous-fluid thermal conductivity ratio parameter. These non-dimensional parameters are introduced as:

$$Da=\frac{K}{L^2},\quad Ra=\frac{\rho_f g\beta\left(T_h-T_c\right)L^3}{\mu_f\alpha_f},\quad H=\frac{h_{fs}L^2}{\varepsilon k_f},\quad K_r=\frac{\varepsilon k_f}{\left(1-\varepsilon\right)k_s} \tag{14}$$

The corresponding non-dimensional form of the boundary conditions is also obtained as:

$$\theta_w=1\quad on\quad X=0,\quad Ypl-Al/2\le Y\le Ypl+Al/2 \tag{15a}$$

$$\theta_w=0\quad \text{on}\quad X=1,\quad Ypr-Ar/2\le Y\le Ypr+Ar/2 \tag{15b}$$

$$\frac{\partial\theta_f}{\partial Y}=\frac{\partial\theta_s}{\partial Y}=0\quad \text{on}\quad D\le X\le 1-D,\quad Y=0,\quad Y=1 \tag{15c}$$

$$\frac{\partial\theta_w}{\partial Y}=0\quad \text{on}\quad 0\le X\le D,\quad 1-D\le X\le 1,\quad Y=0,\quad Y=1 \tag{15d}$$

$$\frac{\partial\theta_w}{\partial Y}=0\quad \text{on}\quad \begin{cases} X=0,\quad 0\le Y\le Ypl-Al/2,\quad Ypl+Al/2\le Y\le 1 \\ X=1,\quad 0\le Y\le Ypr-Ar/2,\quad Ypr+Ar/2\le Y\le 1 \end{cases} \tag{15e}$$

$$\theta_f=\theta_s=\theta_w\quad \text{on}\quad X=D,\quad X=1-D,\quad 0\le Y\le 1 \tag{15f}$$

$$\frac{\partial\theta_f}{\partial X}=R_k\frac{\partial\theta_w}{\partial X}-K_r^{-1}\frac{\partial\theta_s}{\partial X}\quad \text{on}\quad X=D,\quad X=1-D,\quad 0\le Y\le 1 \tag{15g}$$

$$U=V=0\ \text{on}\ X=D,\quad X=1-D,\quad 0\le Y\le 1 \tag{15h}$$

$$U=V=0\ \text{on}\ Y=0,\quad Y=1,\quad \mathrm{D}\le X\le 1-D \tag{15i}$$

where $R_k=K_w/\varepsilon K_f$ is the wall to fluid thermal conductivity ratio parameter. The fluid structure in the cavity is visualized through the definition streamline function as

$$U=\frac{\partial\Psi}{\partial X},\ V=-\frac{\partial\Psi}{\partial Y} \tag{16}$$

The boundary condition of Ψ=0 is imposed at all of the wall surfaces.

The physical quantities of interest are the local Nusselt number for the fluid ($Nu_{f,y}$) and the local Nusselt number for the porous matrix ($Nu_{s,y}$) at the wall interface and the local total heat transfer ($Q_{w,y}$) which occurs at the flash element or radiator.

$$Nu_{f,y} = \left( -\frac{\partial \theta_f}{\partial X} \right)_{X=D,1-D}, \quad Nu_{s,y} = \left( -\frac{\partial \theta_s}{\partial X} \right)_{X=D,1-D}, Q_{w,y} = \left( -\frac{\partial \theta_w}{\partial X} \right)_{X=0,1} \tag{17a}$$

The average value of these physical quantities is also very important as it shows the heat transfer in the cavity. The average Nusselt number of the fluid ($Nu_f$), the average Nusselt number of the porous matrix ($Nu_s$) for the porous phase and the average total heat transfer over the wall containing the flash element or radiator ($Q_w$) are introduced as

$$Q_w = \int_0^1 Q_{w,y} dy, \quad Nu_f = \int_0^1 Nu_{f,y} dy, \quad Nu_s = \int_0^1 Nu_{s,y} dy \tag{17b}$$

It is worth noticing that the average total heat transfer over the wall containing the flash element or radiator ($Q_w$) is indeed the summation of the heat transfer in the porous matrix and the fluid at the wall interfaces. Thus, invoking Eq. (15g), the average total heat transfer ($Q_w$) can be written as

$$Q_w = R_k^{-1} Nu_f + R_k^{-1} K_r^{-1} Nu_s \tag{18}$$

On the other hand, the total average heat transfer through the porous medium by the two channels of the fluid inside the pores and solid structure of the pores from the wall interface can be evaluated as

$$q_t'' = \frac{1}{L} \int_0^L q_{t,y}'' dy = \frac{-1}{L} \int_0^L \left[ \varepsilon k_f \left( \frac{\partial T_f}{\partial x} \right)_{x=d} + (1-\varepsilon) k_s \left( \frac{\partial T_s}{\partial x} \right)_{x=d} \right] dy \tag{19}$$

where $q''_{t,y}$ is the local heat flux at the wall interface. In deriving Eq. (19) it is assumed that the surface porosity is equal to the porous layer porosity. We are also interested in the overall effectiveness of the porous matrix and the fluid in heat transfer. Thus, the total (effective) average Nusselt number of porous media may be introduced as the total average Nusselt

number based on the total heat flux ($q''_t$) and the effective thermal conductivity of the porous matrix and the fluid ($k_{eff}$). In conclusion, using the heat flux introduced in Eq. (19), the total average Nusselt number over the wall is proposed as

$$Nu_t = \frac{q''_t L}{k_{eff}\left(T_h - T_c\right)} = \frac{-1}{\left(K_r + 1\right)} \int_0^1 \left[ K_r \left( \frac{\partial \theta_f}{\partial X} \right)_{X=D} + \left( \frac{\partial \theta_s}{\partial X} \right)_{X=D} \right] dy \tag{20}$$

where $k_{eff} = \varepsilon k_f + (1-\varepsilon)\, k_s$ (see [39]).

## 3. Numerical method and validation

The set of non-dimensional partial differential Eqs. (8)–(13), subjected to the boundary conditions (15a)–(15i), are solved by the Finite Element Method (FEM). In order to employ FEM, the governing equations are first re-written into the weak formulation form [40, 41] and then quadratic elements with Lagrange shape function are applied [40]. The second order discretization for the momentum equation and linear discretization for the heat equations are utilized to discretise the governing equations into a set of algebraic equations. A parallel sparse direct solver [42] and the damped Newton method [41] are utilized to solve the set of the obtained algebraic equations in a fully coupled form. The iterations are repeated to obtain the residuals lower than $10^{-7}$ for all of the equations. The utilized code has been successfully employed to evaluate the results of the previous studies of Lauriat and Prasad [43], Basak et al. [35] and Saeid [16] for the steady state natural convection in an enclosure filled with porous media for the different boundary conditions, as shown in details in Table 1.

**Table 1**

Comparisons of present Nusselt numbers with those represented by previous works

| Case 1 | *Ra* | *Da* | Present results | Lauriat and Prasad [43] |
|---|---|---|---|---|
| Porous cavity, | $10^5$ | $10^{-4}$ | 1.070 | 1.07 |
| $Pr$=1.0, $\varepsilon$=0.4 | $10^6$ | $10^{-4}$ | 2.853 | 2.97 |
| | $10^7$ | $10^{-6}$ | 1.078 | 1.07 |

| | | | | |
|---|---|---|---|---|
| | $10^8$ | $10^{-6}$ | 3.083 | 3.08 |
| Case 2 | *Ra* | *Da* | Present results | Basak et al. [35] |
| Porous cavity, | $10^3$ | $10^{-3}$ | 1.991 | 2.003 |
| *Pr*=7.2, $\varphi$=0˚ | $10^4$ | $10^{-3}$ | 2.031 | 2.030 |
| | $10^5$ | $10^{-3}$ | 3.297 | 3.386 |
| | $10^6$ | $10^{-3}$ | 8.196 | 8.439 |
| Case 3 | *Ra*×*Da* | *D* | Present results | Saeid [16] |
| Conjugate porous | $10^2$ | 0.1 | 2.253 | 2.268 |
| cavity, $K_r$=1 | $10^2$ | 0.5 | 1.167 | 1.178 |
| | $10^3$ | 0.1 | 5.001 | 5.044 |
| | $10^3$ | 0.5 | 1.563 | 1.566 |

In the present study, a non-uniform mesh is utilized to capture the expected high temperature and velocity gradients next to the walls. Each of the porous layer walls are divided into $M \times D$ mesh points, and the part of the horizontal walls which are imposed to the porous medium are divided into $M \times (1-2D)$ mesh points. Thus, the total length of each horizontal wall is divided into M mesh points. The vertical walls are also divided into M mesh points. The mesh points in the porous space are clustered near the walls with the mesh ratio (the largest to smallest element size) of 20. A schematic view of the utilized mesh with the number of mesh points $M$=40 is illustrated in Fig. 3. The number of mesh points in this figure is very low for the sake of graphical illustrations. Significantly larger mesh points were adopted for the calculation of the results. A grid independency check was also performed to ensure the accuracy of the results. The calculations for six different grid sizes and various values of $K_r$ and $R_k$ were performed and the results are summarized in Table 2. The results of Table 2 indicate that both grid sizes of $M$=200 and $M$=250 can provide almost one decimal point of accuracy. As this accuracy is sufficient for most engineering applications and for the purpose of the graphical illustration of the results, the grid size of $M$=200 was selected for the calculations.

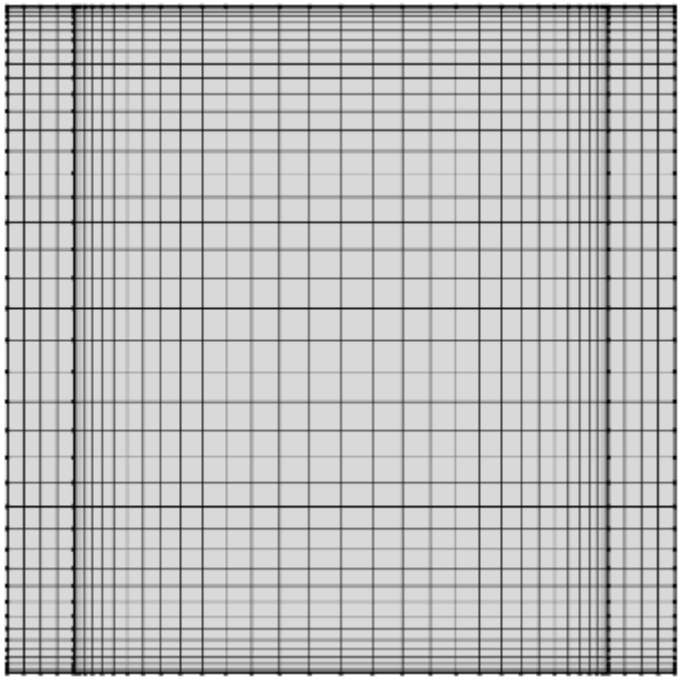

**Fig. 3.** A view of the utilized mesh with $M$=40

**Table 2**

Grid independency test for the values of the average Nusselt number of fluid ($Nu_f$) when $Ra$=$10^6$, $Da$=$10^{-3}$, $Pr$=7.2, $D$=0.1, $H$=10, $\varepsilon$=0.5, $Al$=$Ar$=0.25, $Ypl$=0.8 and $Ypr$=0.2.

| $K_r$ | $R_k$ | M=50 | M=100 | M=150 | M=200 | M=250 |
|---|---|---|---|---|---|---|
| 1 | 1 | 0.732 | 0.731 | 0.728 | 0.726 | 0.727 |
| 1 | 10 | 2.552 | 2.545 | 2.541 | 2.539 | 2.539 |
| 10 | 1 | 0.751 | 0.750 | 0.747 | 0.746 | 0.746 |
| 10 | 10 | 2.627 | 2.619 | 2.616 | 2.614 | 2.614 |

Assuming $Al$=$Ar$=1 and $Ypl$=$Ypr$=0.5 and neglecting the Brinkman effects, the present study is reduced to the study of Saeid [34]. As a comparison, in this case, the results of the present study are compared with the results reported by Saeid [34]. Fig. 4 shows a comparison between the isotherms and streamlines of the present study and those reported in Saeid [34]

when $Ra \times Da = 10^3$, $K_r = 100$, $D = 0$, $H = 1$ and $R_k = 1$. The average Nusselt number for the fluid ($Nu_f$) and porous matrix ($Nu_s$), the total heat transfer ($Q_w$) and the absolute maximum value of the streamline function ($|\Psi|_{max}$) evaluated in the present study are compared with those reported by Saeid [34] in Table 3. Fig. 5 also as a comparison with the results of Saeid [34] depicts the average Nusselt number in the fluid phase ($Nu_f$) and porous matrix phase ($Nu_s$) as a function of the porous-fluid thermal conductivity ratio parameter ($K_r$). As seen, the results of Figs. (4) and (5) as well as Table 3 show good agreement with the previous study.

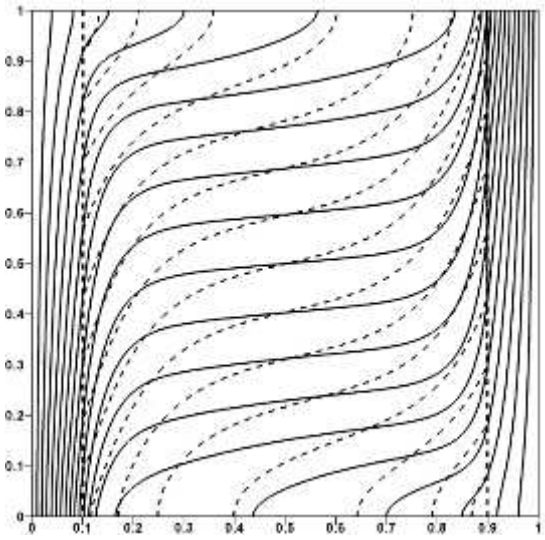

Isotherms (present study)

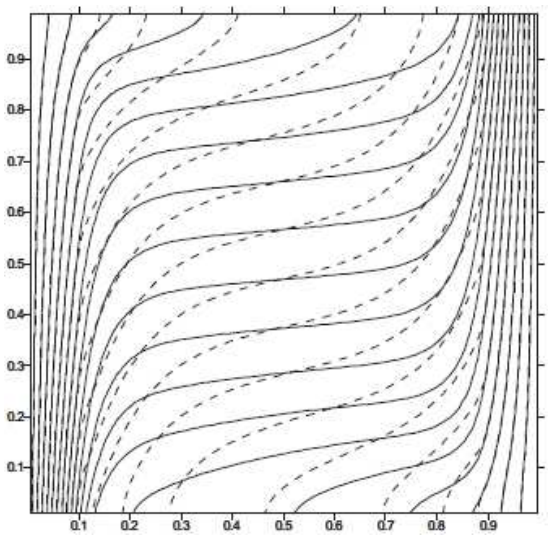

Isotherms (Saeid [34])

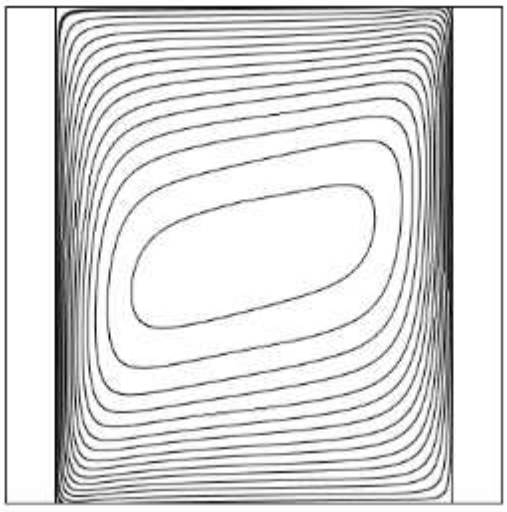

Streamlines (present study)

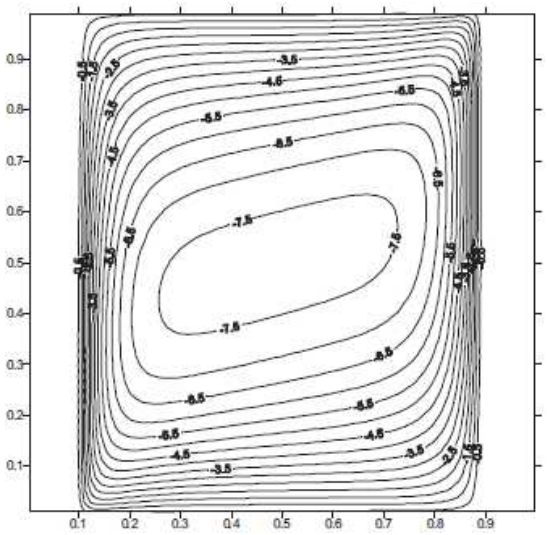

Streamlines (Saeid [34])

**Fig. 4.** A comparison between the results of Saeid [34] and the results of the present study in the case of $D$=0.1, $R_k$=1, $H$=1, $K_r$=100, $Ra \times Da$=$10^3$, and $\Delta\theta$=0.05.

**Table 3**

Comparison of the results reported by Saeid [34] and the results of the present study

| | $K_r$ | $D$=0.1, $R_k$=1.0, $H$=1.0 and $Ra \times Da$=$10^3$ | | | |
|---|---|---|---|---|---|
| | | $Nu_f$ | $Nu_s$ | $Q_w$ | $\lvert\Psi\rvert_{max}$ |
| Present results | 0.1 | 1.252 | 0.268 | 3.930 | 7.458 |
| | 10 | 3.205 | 0.552 | 3.260 | 8.033 |
| | 100 | 3.243 | 1.066 | 3.253 | 7.993 |
| Saeid [34] | 0.1 | 1.189 | 0.260 | 3.787 | 7.252 |
| | 10 | 3.113 | 0.535 | 3.166 | 7.750 |
| | 100 | 3.150 | 1.030 | 3.160 | 7.708 |

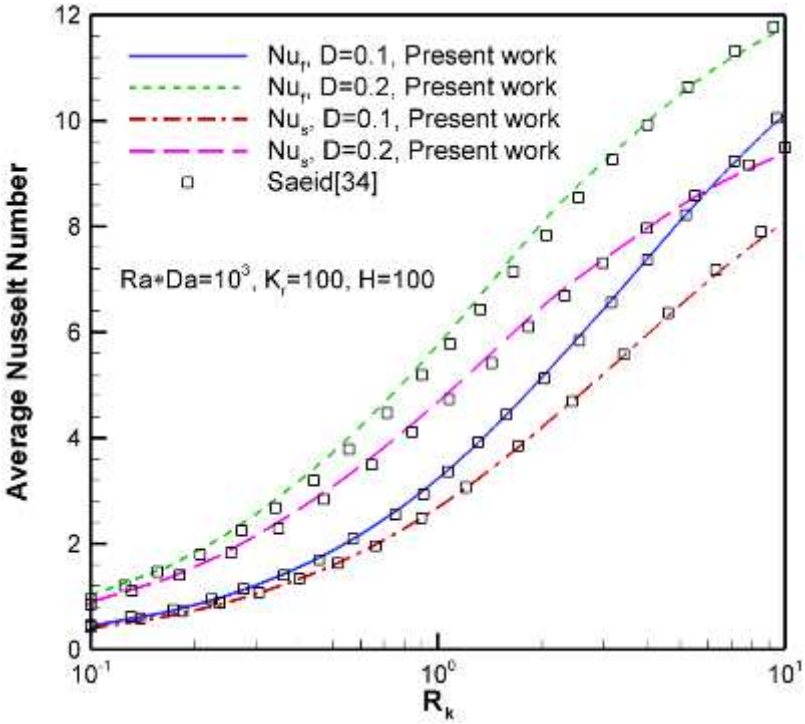

**Fig. 5.** Variation of average Nusselt Numbers with $Ra$ for selected values of parameter $K_r$: a comparison between the results of Saeid [34] and the results of the present study.

## 4. Results and discussion

In this section, the results illustrate the effect of the different positions of hot and cold elements on flow and thermal field in an enclosure under both local thermal non-equilibrium (LTNE) and local thermal equilibrium (LTE) models. In addition, the effects of the variation of the dimensionless parameters on the different average Nusselt numbers have been studied for the nine cases of thermally active locations, depicted in Fig. 2. The values of the dimensionless parameters, including the Rayleigh number ($Ra$), the Darcy number ($Da$), the Prandtl number ($Pr$), the wall thickness to height ratio ($D$), the porous-fluid thermal conductivity ratio parameter ($K_r$), the wall to fluid thermal conductivity ratio parameter ($R_k$), and the porous-fluid interface convection parameter ($H$) are studied. The results of the present study are reported for the range of the non-dimensional parameters as: $10^3 \leq Ra \leq 10^7$, $10^{-5} \leq Da \leq 10^{-1}$, $0.026 \leq Pr \leq 1000$, $0.01 \leq D \leq 0.4$, $0.1 \leq K_r \leq 1000$, $0.1 \leq R_k \leq 10$, $0.1 \leq H \leq 1000$, while the porosity and the dimensionless height of the flash element and the radiator are kept constant (i.e., $\varepsilon$=0.5, $Al$=$Ar$=0.25).

### 4.1. Effect of thermally active locations on flow and thermal fields

In order to investigate the effect of the heating and cooling locations on the natural convection heat transfer, all other dimensionless parameters are maintained constant at $Ra$=$10^6$, $Da$=$10^{-3}$, $Pr$=7.2, $D$=0.1, $R_k$=1, $K_r$=1, $H$=1 and the nine cases of different thermally active locations, illustrated in Fig. 2, are considered. Fig. 6 demonstrates the flow pattern and

temperature distributions of the fluid and the solid phases of the porous medium in terms of the streamlines and isotherms contours. It is observed from Fig. 6 that the partially heating and cooling locations have a significant influence on the isotherms and streamlines inside the enclosures. The average Nusselt number for the solid ($Nu_s$) and fluid ($Nu_f$) as well as average heat transfer through the walls ($Q$) and the absolute maximum stream function ($\left|\Psi\right|_{\max}$) have been reported in the legend of each figure.

The results interestingly demonstrate that there exists a relation between the results of the specific each pair of the nine selected cases of the elements locations. This relation is such that by rotating the position of the elements through 180 degrees about the origin, the average Nusselt number for the fluid phase inside the pores and solid structure of the pores (the pores porous medium phase), the average heat transfer through the walls and the absolute maximum stream function almost will not change (i.e. case (a) and (i), case (b) and (f), case (d) and (h)). Moreover, considering the 180 degree of the rotation about the origin, the contours of the isotherms and the streamlines of each of the pairs show similar patterns. However, the results of the cases (c) and (g) do not follow this conclusion. Fig. 6 shows also that the core region of the rotating cell of the streamlines of case (g) splits into two almost separate parts next to the heating and cooling zones in the top and bottom areas of the enclosure, respectively. Indeed, the hot element in the top heats its surrounding regions. The hot fluid tends to move upward and above the element. Similarly, the cold radiator sinks the heat and cools its surrounding regions. The cold fluid tends to settle down next to the bottom of the cavity. Therefore, the hot fluid is trapped in the top regions and the cold fluid is also trapped in the bottom regions. In this case, the heat transfer occurs due to diffusion mechanism in the core section of the cavity where the hot and cold fluids are in neighbourhood. Due to the heat transfer between the hot and cold regions in the core area smooth natural convection in the top and bottom regions can be seen. Attention to other cases shows that the dual inner cells do not occur in the other cases

of thermally active locations. Attention to the effect of the position of the element on the heat and flow patterns shows as the position of the hot element shifts into the bottom and the cooling radiator shifts upward into the top the flow strength and heat transfer increases. Hence, as substantiated in Fig. 6, the maximum flow strength occurs for case (c).

Although the strength of the fluid circulation of the case (c) is more than all cases, when the elements are located at the middle (i.e. case (e)), more heat will be carried out by the fluid through the porous region due to highest average Nusselt number for the fluid among the other cases. This is due to the contribution of the porous space and heat channelling in the porous matrix. Indeed, in the case (e) the distance between the hot element and the radiator is minimum. Furthermore, the lowest rate of heat transfer in the enclosure is belonging to the case (g) due to the discussed flow patterns and the longest distance between the hot element and the cold radiator. The labelled results of the average Nusselt numbers and the average heat transfer through the walls presented in legends of Fig. 6 demonstrate that Eq. (18) holds true, which confirms the correct implementation of the LTNE boundary condition at the interface of solid wall and the porous media.

In order to compare heat transfer and fluid flow mechanisms in porous medium for both models of LTE and LTNE, the isotherms and streamlines for the case of LTE model are exhibited in Fig. 7. The results of Fig. 7 are calculated for the same set of non-dimensional parameters as those reported for Fig. 6. Comparison between the results of Figs. 6 and 7 indicates that the patterns of the isotherms in the solid walls and porous region as well as the streamlines in the porous region are comparatively similar in both of LTNE and LTE models. Also, the aforementioned coordination between the cases in the LTNE model is established here for those pair cases in the LTE model. Another point that can be drawn from the comparison between Figs. 6 and 7 is that the values of average Nusselt numbers of porous and walls domain under LTE model are higher than that under LTNE model. Therefore, under

identical boundary condition, the amount of heat that is transported through the porous medium under the LTE model is higher than that under the LTNE model at considered values of dimensionless parameters. This is due to the fact that at high values of thermal equilibrium parameters ($K_r$=100, $H$=100), the values of average Nusselt numbers related to LTE and LTNE models are identical, where the average Nusselt number for the fluid phase inside the pores of the porous matrix represent the maximum possible [34]. However, the values of absolute maximum stream function for the case of LTE model are lower than that of the LTNE model.

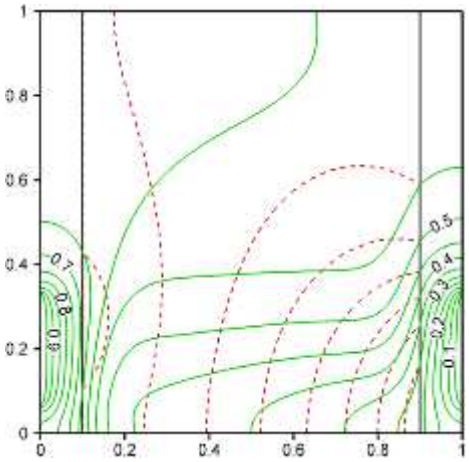

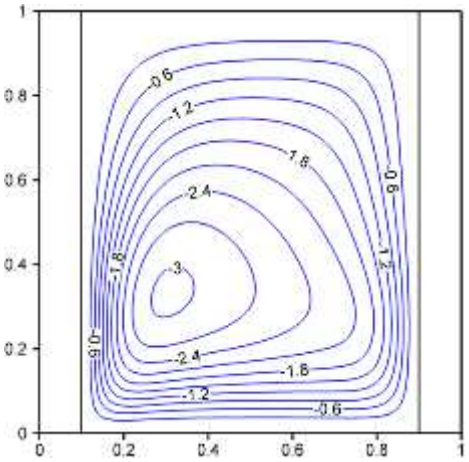

(a)

$Nu_f = 0.925,\ Nu_s = 0.219,\ Q_w = 1.144$ $\quad\quad$ $|\Psi|_{\max} = 3.060$

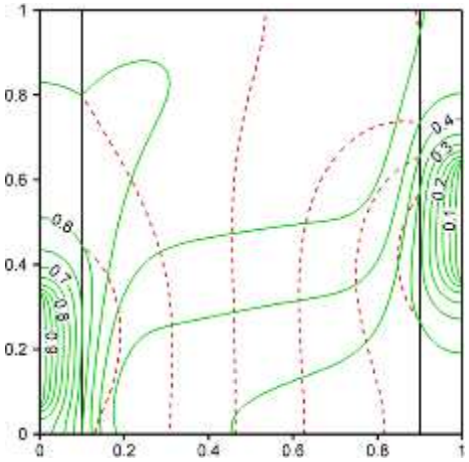

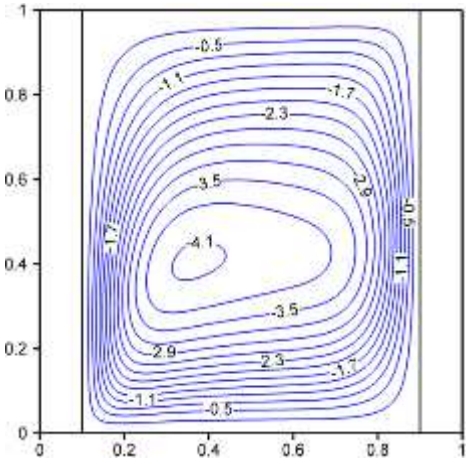

(b)

$Nu_f = 0.996,\ Nu_s = 0.254,\ Q_w = 1.250$ $\qquad$ $|\Psi|_{\max} = 4.143$

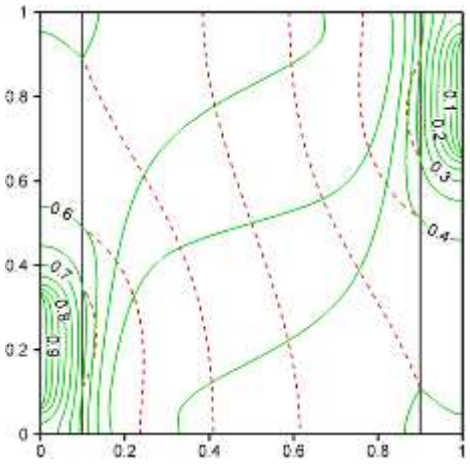

(c)

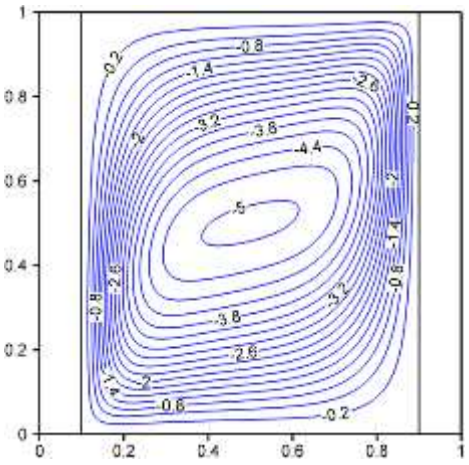

$Nu_f = 0.916,\ Nu_s = 0.266,\ Q_w = 1.183$ $\qquad$ $|\Psi|_{\max} = 5.050$

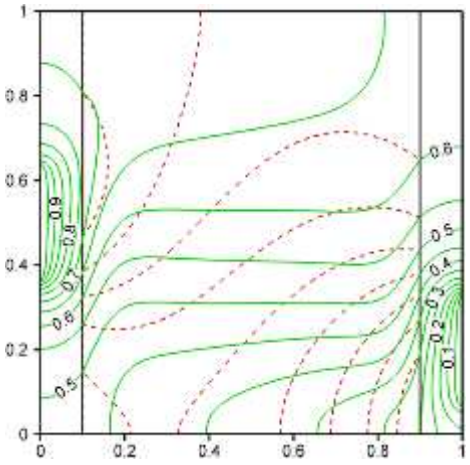

(d)

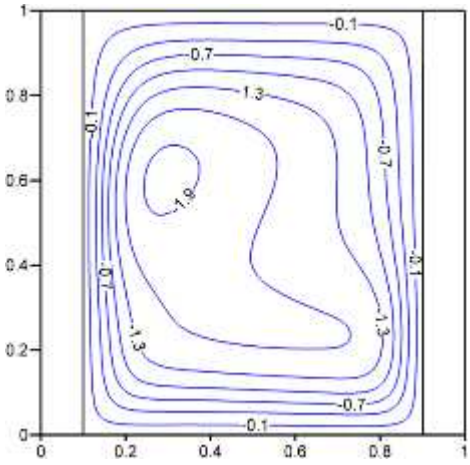

$Nu_f = 0.916,\ Nu_s = 0.198,\ Q_w = 1.114$ $\qquad$ $|\Psi|_{\max} = 1.977$

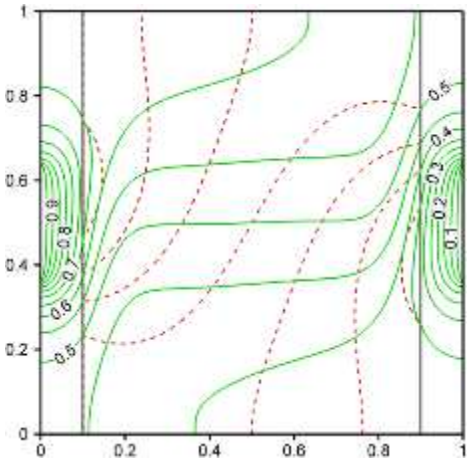

(e)

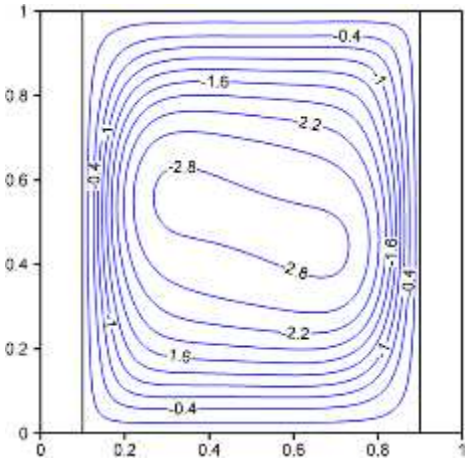

$Nu_f = 1.055,\ Nu_s = 0.235,\ Q_w = 1.290$

$|\Psi|_{\max} = 2.874$

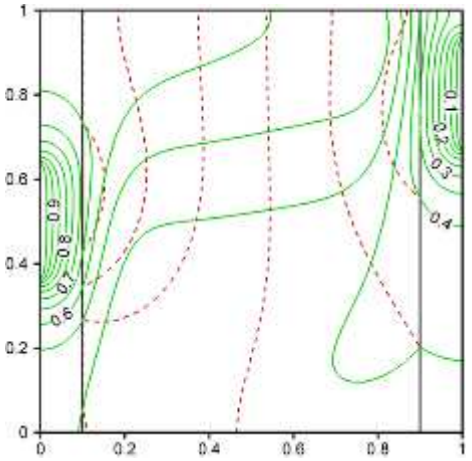

(f)

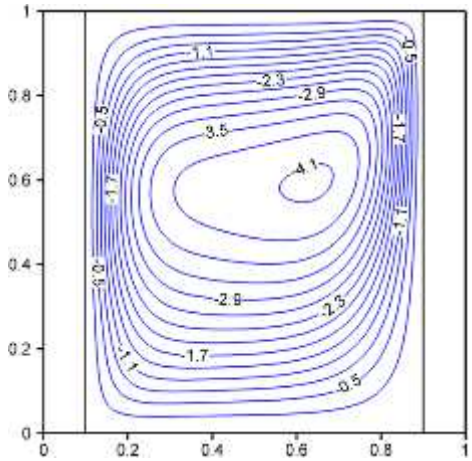

$Nu_f = 0.998,\ Nu_s = 0.252,\ Q_w = 1.250$

$|\Psi|_{\max} = 4.143$

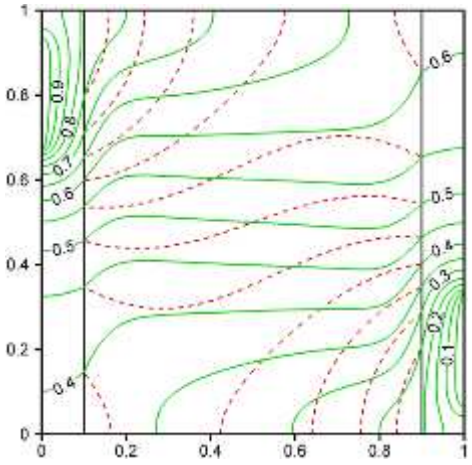

(g)

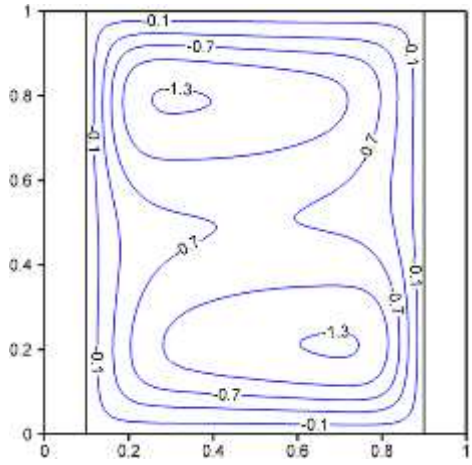

$Nu_f = 0.751,\ Nu_s = 0.168,\ Q_w = 0.919$ $\qquad$ $|\Psi|_{\max} = 1.325$

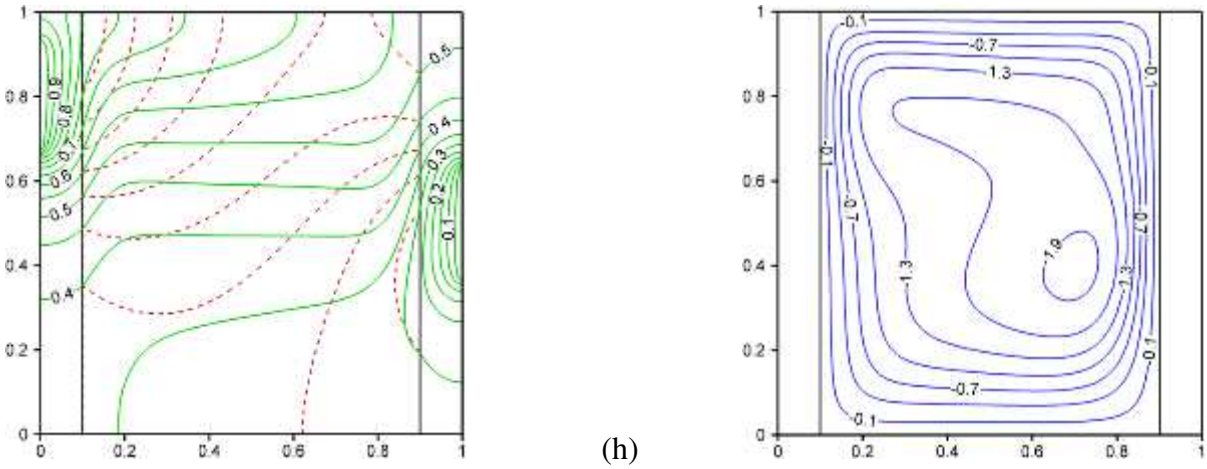

(h)

$Nu_f = 0.918,\ Nu_s = 0.196,\ Q_w = 1.114$ $\qquad$ $|\Psi|_{\max} = 1.977$

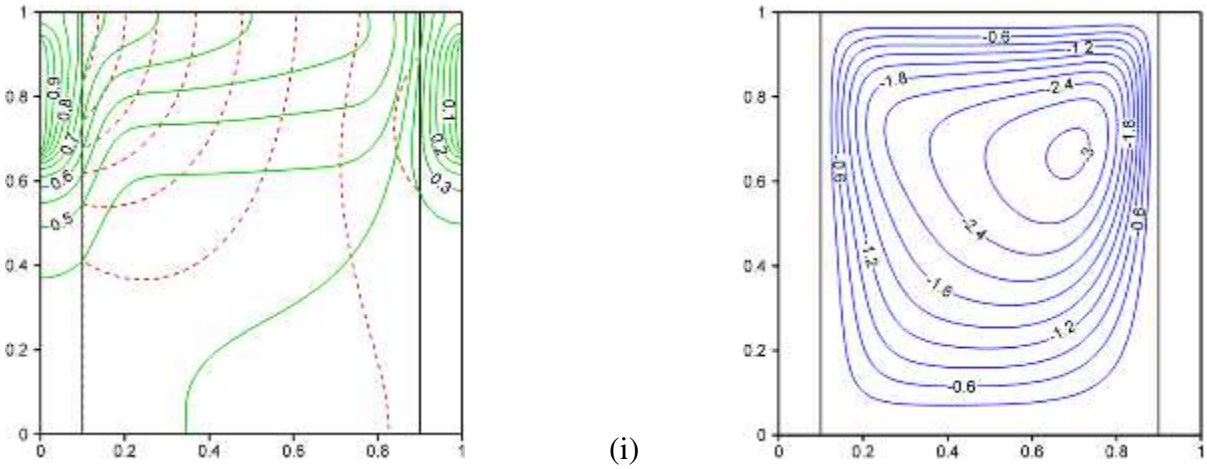

(i)

$Nu_f = 0.929,\ Nu_s = 0.215,\ Q_w = 1.144$ $\qquad$ $|\Psi|_{\max} = 3.060$

**Fig. 6.** (left) Isotherms (solid green line for $\theta_f$ , dashed red line for $\theta_s$ ) and (right) streamlines at $Ra = 10^6$, $Da = 10^{-3}$, $Pr = 7.2$, $\varepsilon = 0.5$, $D = 0.1$, $H = 1$, $K_r = 1$, $R_k = 1$ and $\Delta\theta = 0.05$ for different thermally active locations (case a ~ case i).

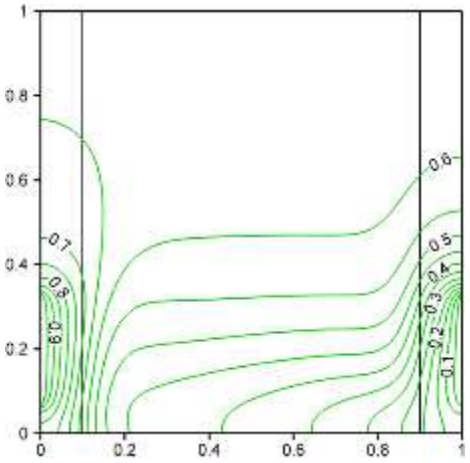

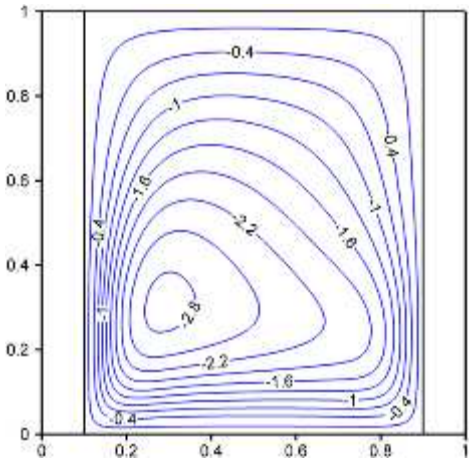

(a)

$Nu_f = 1.084,\ Q_w = 1.084$ $\quad |\Psi|_{\max} = 2.892$

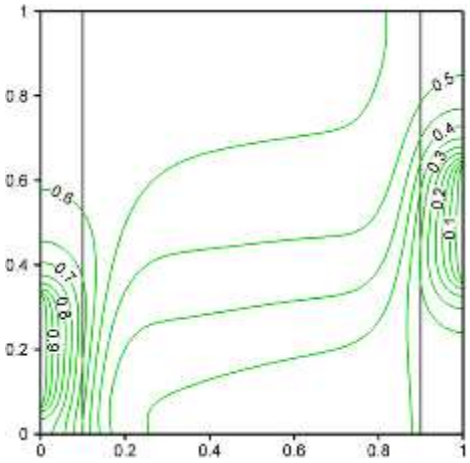

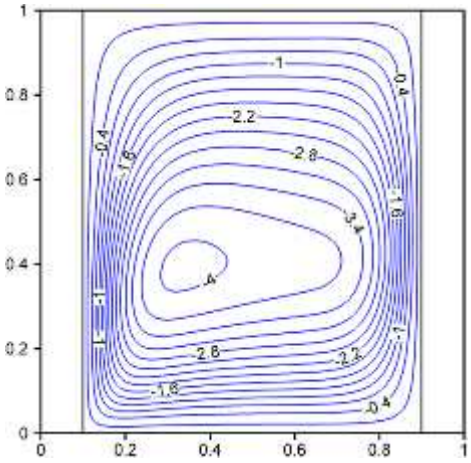

(b)

$Nu_f = 1.216,\ Q_w = 1.216$ $\quad |\Psi|_{\max} = 4.078$

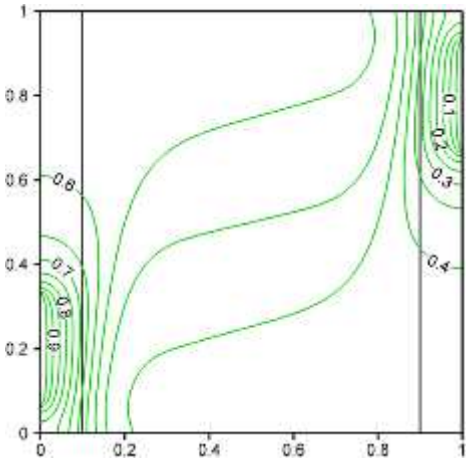

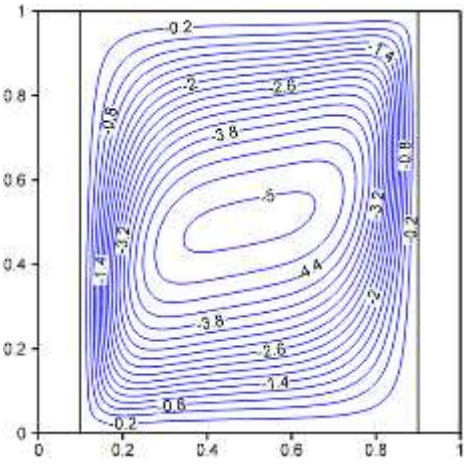

(c)

$Nu_f = 1.153,\ Q_w = 1.153$ $\quad |\Psi|_{\max} = 5.076$

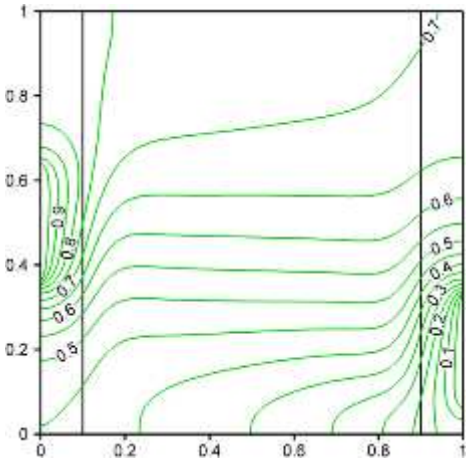

(d)

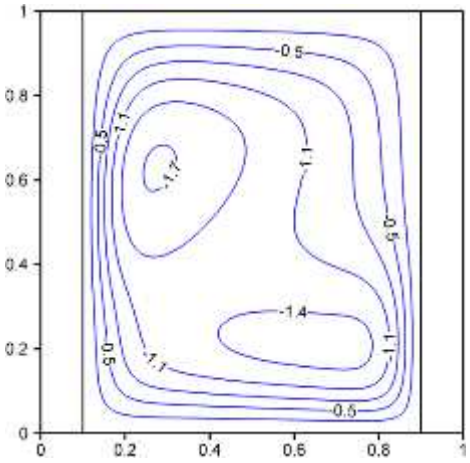

$Nu_f = 1.007,\ Q_w = 1.007$ $\quad |\Psi|_{\max} = 1.736$

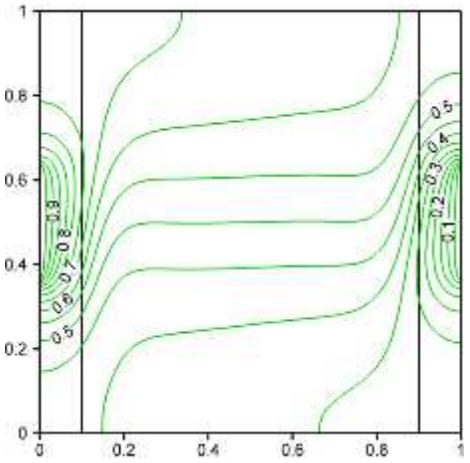

(e)

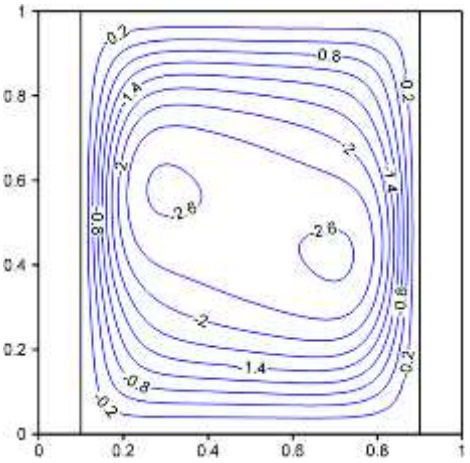

$Nu_f = 1.243,\ Q_w = 1.243$ $\quad |\Psi|_{\max} = 2.648$

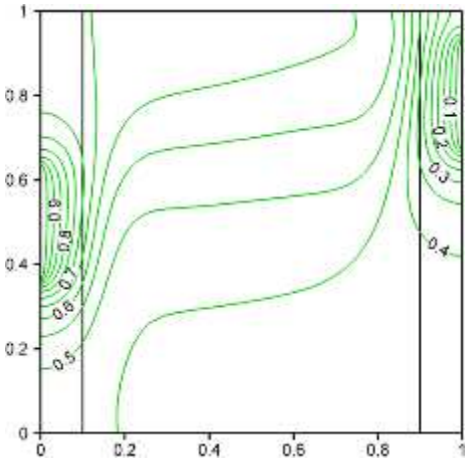

(f)

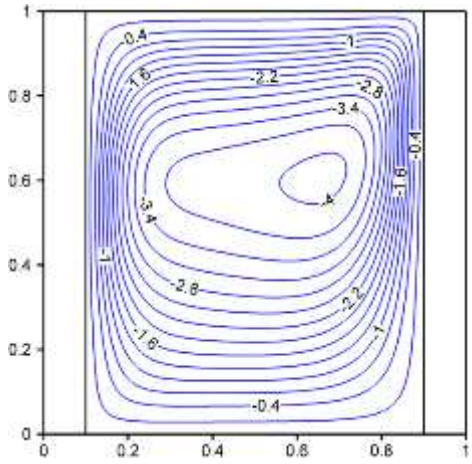

$Nu_f = 1.215,\ Q_w = 1.215$ $\quad |\Psi|_{\max} = 4.078$

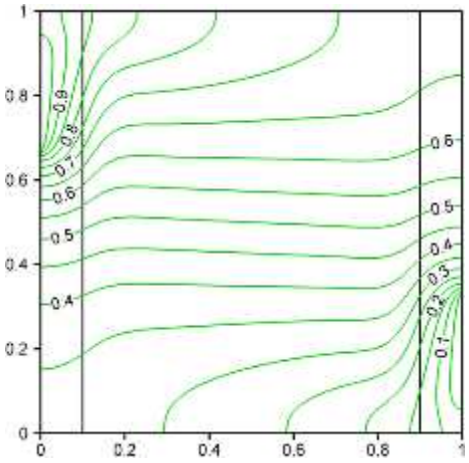

(g)

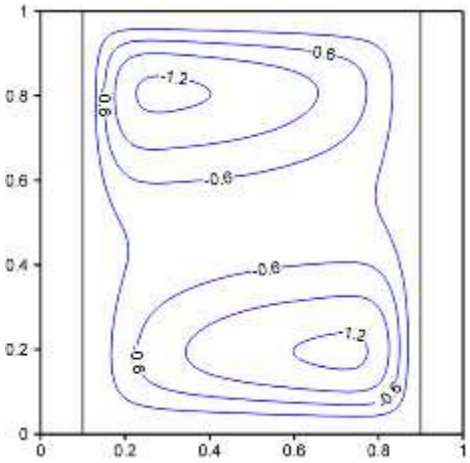

$Nu_f = 0.757,\ Q_w = 0.757$

$|\Psi|_{\max} = 1.259$

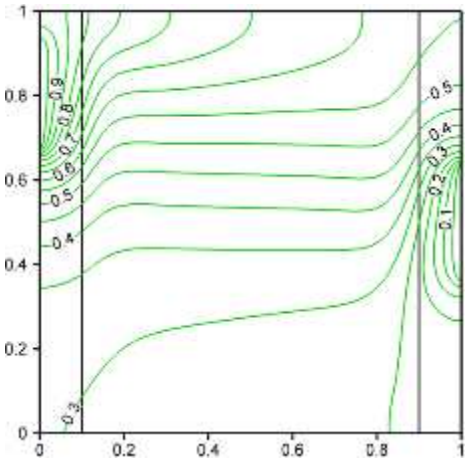

(h)

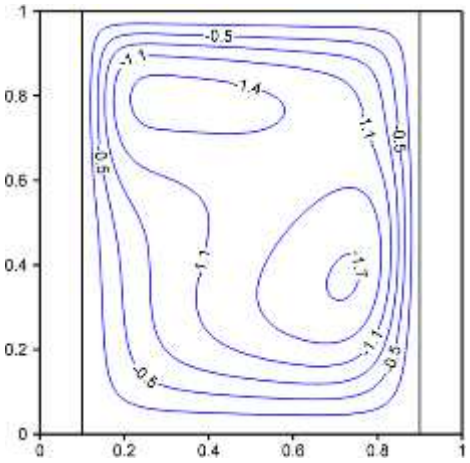

$Nu_f = 1.007,\ Q_w = 1.007$

$|\Psi|_{\max} = 1.736$

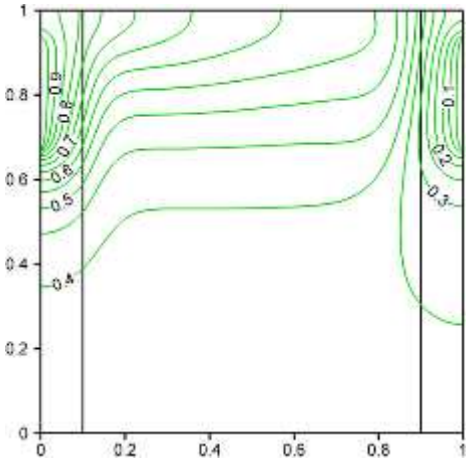

(i)

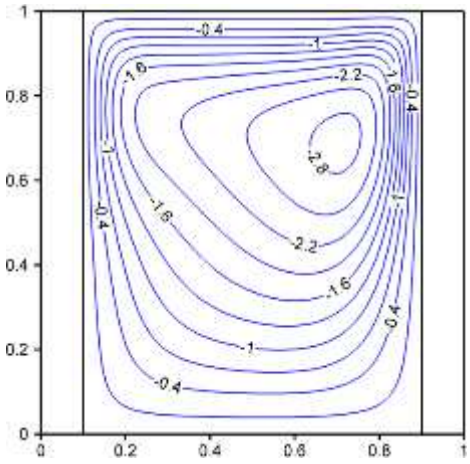

$Nu_f = 1.083,\ Q_w = 1.083$

$|\Psi|_{\max} = 2.892$

**Fig. 7.** (left) Isotherms and (right) streamlines at $Pr$=7.2, $\varepsilon$=0.5, $D$=0.1, $R_k$=1, $Ra$=$10^6$, $Da$=$10^{-3}$ and $\Delta\theta$=0.05 for different thermally active locations (case a ~ case i) under LTE.

### 4.2. Effect of variations parameters on average Nusselt numbers for different thermally active locations

The substantial quantity of practical interest in natural convection problems is the average Nusselt number which quantifies the amount of heat injected or sunk from the partially heated or cooled walls. The influence of the thermally active locations on the heat transfer rate via the average Nusselt number in the porous region has been investigated in this sub-section for different values of the Darcy numbers ($Da$), the Rayleigh numbers ($Ra$), the porous-fluid interface convection parameter ($H$), the porous-fluid thermal conductivity ratio parameters ($K_r$), the wall to fluid thermal conductivity ratio parameters ($R_k$), the wall thickness to height ratios ($D$), and the Prandtl numbers ($Pr$). The results are described as follows:

Fig. 8 shows the variation of average Nusselt number for the fluid phase (in the pores) and the solid phase (solid structure of the pores), as a function of Darcy number ($Da$) for all of the nine studied cases of thermally active locations at fixed $D$=0.1, $K_r$=1, $R_k$=1, $Ra$=$10^6$, $Pr$=7.2, and $H$=1. Fig. 8a and 8b illustrate the average Nusselt number for the fluid phase and the porous phase, respectively. An overview of Figs. 8a and b reveal that the average Nusselt number is an increasing function of Darcy number ($Da$) for the fluid phase ($Nu_f$) and a decreasing function of $Da$ for the solid phase of the porous matrix ($Nu_s$) for all of the elements configurations. This behaviour can be related to the transition of the heat transfer mechanism from the conduction dominated regime for the low $Da$ to convection dominated regime for high $Da$ due to the increasing permeability of the porous medium. The variations of both of the average Nusselt numbers, i.e. $Nu_f$ and $Nu_s$, with $Da$ are associated with a large slop until $Da$=$10^{-3}$, after that the intensity of variations becomes weak.

As can be seen from these figures, the heat transfer rate by both fluid and solid phases for all symmetrical pairs of cases, which were assessed in the previous sub-section, are almost identical. It is very obvious that the heat transfer by fluid for the case of middle-middle heating and cooling (i.e. case (e)) provides a better heat transfer rate compared to other cases of thermally active locations within the whole range of *Da*. Considering high values of Darcy Number, the poorest heat transfer rate by fluid is related to case (g), which the partial heating and cooling are located at top and bottom part of walls, respectively, as shown in Fig. 8a. Furthermore, the highest and lowest rate of heat transfer by solid phase in porous region belongs to the cases (c) and (g), respectively, as shown in Fig. 8b. However, considering the small value of Darcy number ($Da$=$10^{-4}$), some exceptional trend of behaviour for some configurations can be seen. These exceptional behaviours are mostly due to the contribution of the heat changeling in the porous matrix.

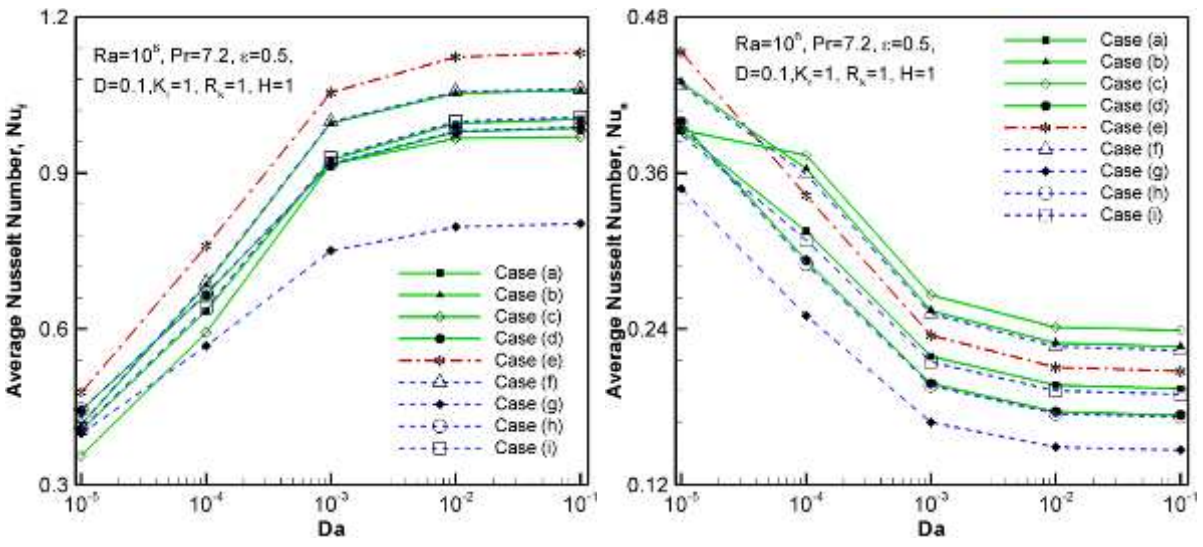


(a) Fluid phase (b) Solid phase

**Fig. 8.** Variation of $Nu_f$ and $Nu_s$ with *Da* for different thermally active locations.

Fig. 9 illustrates the variation of the average Nusselt number for both of the fluid and porous phases as a function of Rayleigh number ($Ra$) for various case of element locations when $D = 0.1$, $K_r = 1$, $Da = 10^{-3}$, $Pr = 7.2$, $R_k = 1$, and $H = 1$. In general, $Nu_f$ increases and $Nu_s$ reduces continually with an increase of $Ra$ for all selected cases. In fact, the increase of the Rayleigh number boosts the buoyancy forces and tends to induce a stringer convective heat transfer regime in the fluid phase. In particular, when $Ra>10^4$, the values of both $Nu_f$ and $Nu_s$ change steeply for all of the cases of (a) – (i). Indeed, the case of $Ra=10^4$ ($Ra\times Da=10$) is where the convection mechanism becomes important and the increase of the Rayleigh number significantly increases the heat transfer. However, there are some exceptions, which indicate that the average Nusselt numbers strongly depend on the location of the elements. For example, considering case (c), in which the bottom is heating and top is cooling, $Nu_s$ increases with increasing $Ra$ until $10^5$. Afterwards, it decreases steeply in the range of $10^5<Ra<10^7$, which has the highest heat transfer rate in this range in comparison to the other considered cases, as shown in Fig. 9b. It is observed from Fig. 9a that the heat transfer rate by the fluid phase of the case (e) is greatest among the other cases. Moreover, the case (g) shows the least heat transfer rate for both fluid and solid phases of the porous medium.

In order to perform the more comprehensive investigation of the effect of different thermally active locations on heat transfer in the porous enclosure, Figs. 10 and 11 are prepared to show the variation of total average Nusselt number with the Rayleigh number for different values of $K_r$ (0.1 and 100) and $R_k$ (0.1 and 10). Generally, these figures demonstrate that the total average Nusselt number increases when the Rayleigh number is increased for all of the cases of the walls mounted elements. In addition, the heat transfer rate inside the porous medium increases with the raise of $K_r$ and $R_k$. A close look at these figures reveals that the total average Nusselt number is almost independent of the Rayleigh number in the range of $10^3<Ra<10^5$ for $K_r=0.1$ and $R_k=0.1$ (see Figs. 10a and 11a), and in the range of $10^3<Ra<10^4$

for $K_r$=100 and $R_k$=10 (see Figs. 10b and 11b) due to the domination of the conduction heat transfer inside the porous layer. Moreover, the difference in the total average Nusselt number among different cases of thermally active locations increases when the Rayleigh number is increased for the high values of $K_r$ and $R_k$. It can ~~be~~ clearly be seen from Figs. 10 and 11 that the case (e) shows the maximum heat transfer rate, and the case (g) corresponds to the minimum heat transfer rate within the whole range of the studied Rayleigh numbers for both low and high values of $K_r$ and $R_k$.

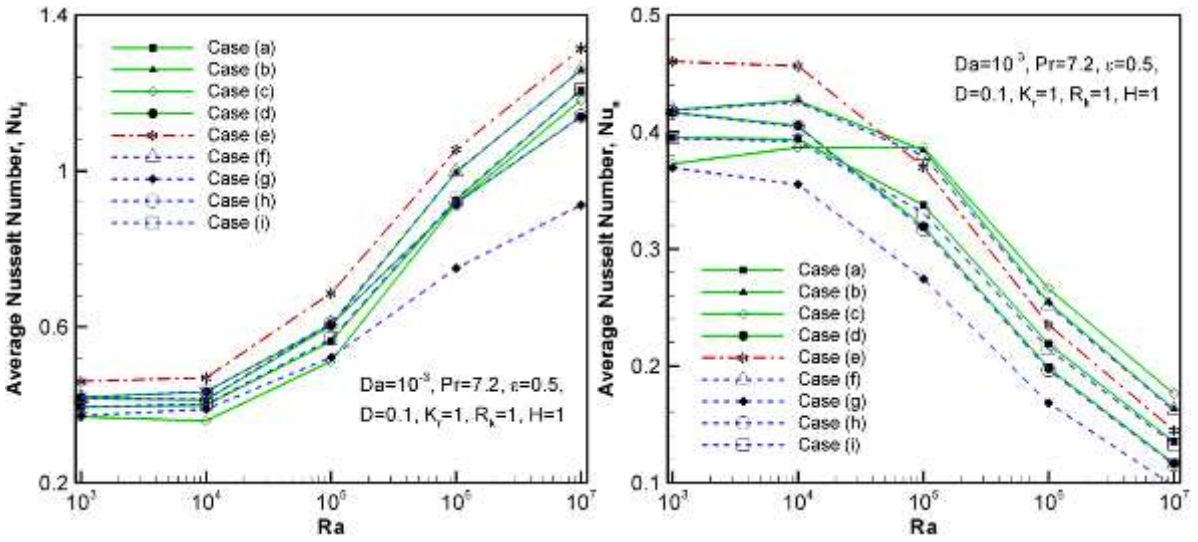


(a) Fluid phase (b) Solid phase

**Fig. 9.** Variation of $Nu_f$ and $Nu_s$ with $Ra$ for different thermally active locations.

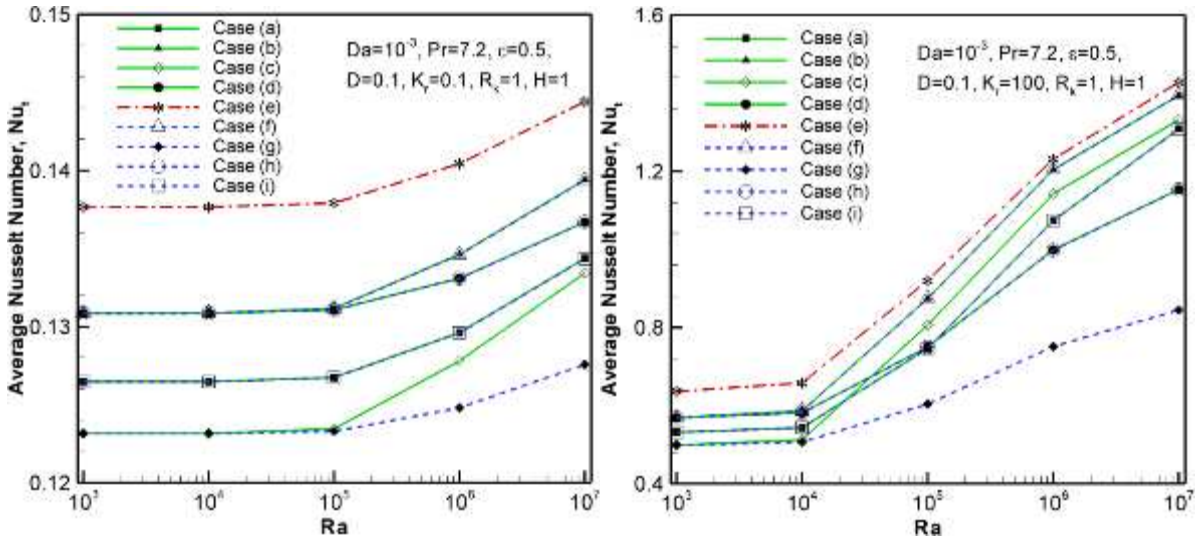


(a) $K_r$=0.1 (b) $K_r$=100

**Fig. 10.** Variation of $Nu_t$ with $Ra$ for different elements locations and two values of $K_r$.

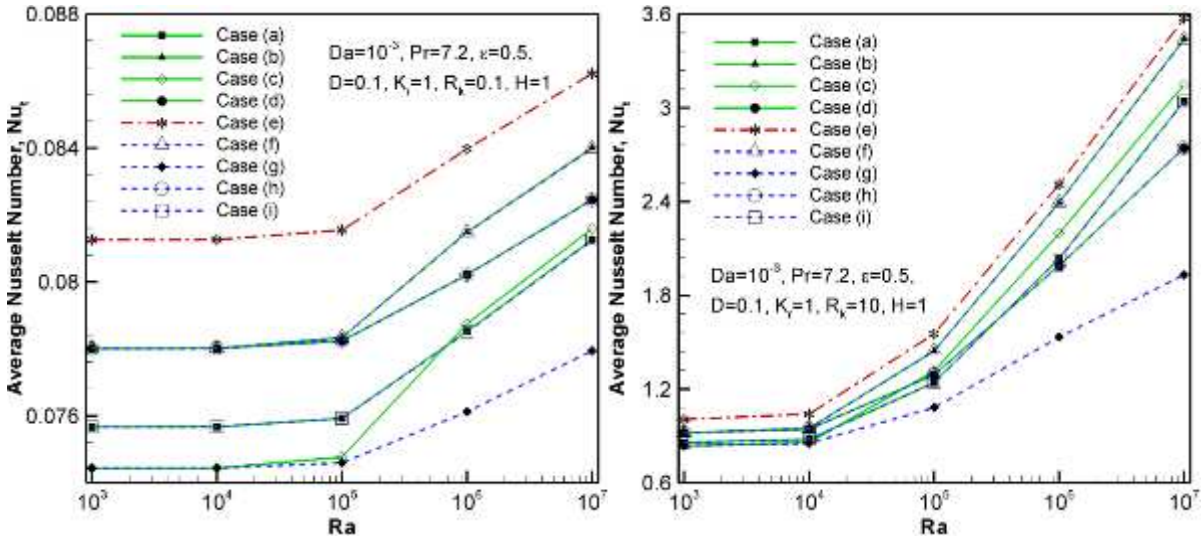


(a) $R_k$=0.1 (b) $R_k$=10

**Fig. 11.** Variation of $Nu_t$ with $Ra$ for different thermally active locations.

Fig. 12 demonstrates the influence of the porous-fluid thermal conductivity ratio parameter ($K_r$) on the total average Nusselt number ($Nu_t$) for different cases of thermally active locations at fixed $Pr$=7.2, $\varepsilon$=0.5, $D$=0.1, $Ra$=$10^6$, $Da$=$10^{-3}$, $R_k$=1, and $H$=1. It is observed from Fig. 12 that the values of the total average Nusselt number through the porous layer, i.e. fluid and porous matrix, are increasing steeply with the increase in $K_r$ from 0.1 to 10, after which the variations are increasing with less slope until $K_r$=100, and they finally ~~they~~ become approximately constant from 100 to 1000. The increase of $K_r$ shows the increase of the thermal conductivity of the fluid compared to the porous matrix. Therefore, the enhancement of heat transfer due to convective mechanism can be expected. According to Fig. 12, the difference in the values of the total average Nusselt numbers among different cases of thermally active locations increase with increasing $K_r$. Furthermore, the values of the total average Nusselt number of each of the symmetrical pairs of selected cases (i.e. cases (a) and (i), cases (b) and (f), cases (d) and (h)) are identical. As expected from previous results, the cases (e) and (g) respectively show the highest and lowest rate of heat transfer inside the porous medium in comparison to other cases of thermally active locations for all the studied ranges of $K_r$.

Fig. 13 displays the effect of the wall to fluid thermal conductivity ratio parameter ($R_k$) on the total average Nusselt number ($Nu_t$) for $Ra$=$10^6$, $Da$=$10^{-3}$, $Pr$=7.2, $\varepsilon$=0.5, $D$=0.1, $K_r$=1, $H$=1 and different elements locations. As seen, the heat transfer rate through porous layer for all cases of thermally active locations increases monastically with augmentation of $R_k$, and in particular, increases steeply in the range $R_k$>1. This is because at high values of $R_k$, the walls have high thermal conductivity, which leads to low thermal resistance. Hence, the temperature difference across the left and right faces of the porous layer increases due to the good conductive walls. Therefore, the rate of heat transfer in the porous domain increases with the increase in $R_k$. In addition, it is clear that the locations of the partial heating element and cooling radiator have no significant effect on the total heat transfer rate due to the high thermal

resistance of walls at low values of $R_k$ (i.e. $R_k$=0.1). In addition, the influence of elements locations on the rate of the total heat transfer boosts as $R_k$ increases. The total average Nusselt number for cases (e) and (g) respectively reaches the maximum and the minimum value within the entire range of $R_k$.,

The effect of the porous-fluid interface convection parameter ($H$) on the total average Nusselt number ($Nu_t$) for all of the considered arrangements of partial heating and cooling at fixed $Ra$=$10^6$, $Da$=$10^{-3}$, $Pr$=7.2, $\varepsilon$=0.5, $D$=0.1, $K_r$=1, and $R_k$ =1 is studied, and the results are depicted in Fig. 14. Based on the results of this figure, the total average Nusselt number ($Nu_t$) is an increasing function of $H$, especially for large values of $H$. It is also evident that the increase of $H$ enhances the thermal interaction between the fluid in the pores (fluid phase) and the solid structure of the pores (porous phase), and consequently, it tends to detract the temperature difference between two phases during the transfer process. Hence, the total of heat transfer rate boosts with the increase of $H$. Once again, we see coincidence of the results of each symmetrical pair of considered cases in all ranges of $H$. The maximum and minimum total heat transfer occurs for cases (e) and (g), respectively, as shown in Fig. 14. Via the blockage circulation formation in the top and bottom regions of the cavity, the case (g) corresponds to the lowest heat transfer rate.

Fig. 15 presents the effect of the wall thickness to height ratio ($D$) on the total average Nuseelt number ($Nu_t$) in the porous region for the different cases of the thermally active locations at fixed $Ra$=$10^6$, $Da$=$10^{-3}$, $Pr$=7.2, $\varepsilon$=0.5, $K_r$=1, $R_k$=1, and $H$=1. Increasing the wall thickness ($D$) dominates the conduction mode in the system. This is due to the solid walls that behave as insulated materials in this case. Therefore, the total average Nusselt number of the porous medium for all cases reduces steadily with thickening of the walls, where this reduction is more pronounced in the range $0.01<D<0.1$, as shown in Fig. 15. The heat transfer rate for all cases of thermally active locations strongly depends on the walls' thickness, so that the

arrangement of considered cases based on heat transfer rate is significantly different at each investigated value of $D$. Nevertheless, the cases (e) and (g) have the highest and lowest total average Nusselt number within the porous domain, compared to other cases of the elements locations for all studied ranges of $D$. Although, for low values of $D$ (<0.1), the values of the total average Nusselt number for the symmetrical pairs cases of (b) and (f) are approximately identical with case (e), as shown in Fig. 15.

Finally, Fig 16 shows the variation of the total average Nusselt number ($Nu_t$) with the Prandtl number ($Pr$) for the different cases of the thermally active locations at fixed $Ra$=$10^6$, $Da$=$10^{-3}$, $D$=0.1, $K_r$=100, $R_k$=10, and $H$=100. The results have been presented for the values of $Pr$=0.026 (molten metal), $Pr$=7.2 (salt water), and $Pr$=1000 (oil). As ~~it~~ can be seen from Fig. 16, the heat transfer rate increases with increasing $Pr$ until $Pr$=7.2, then remains constant with the further increase of $Pr$ for all the partially heating and cooling cases. This behaviour is attributed to the fact that at high values of $Pr$, the viscous diffusion rate is larger than the thermal diffusion rate and consequently, the convection is more effective in transferring heat in comparison to pure conduction, therefore; the total average Nusselt number is high in such cases. Moreover, it is evident that the case (e) offers an enhanced heat transfer rate within the entire range of $Pr$, while case (g) with a large difference with other cases corresponds to the lowest level of heat transfer rate.

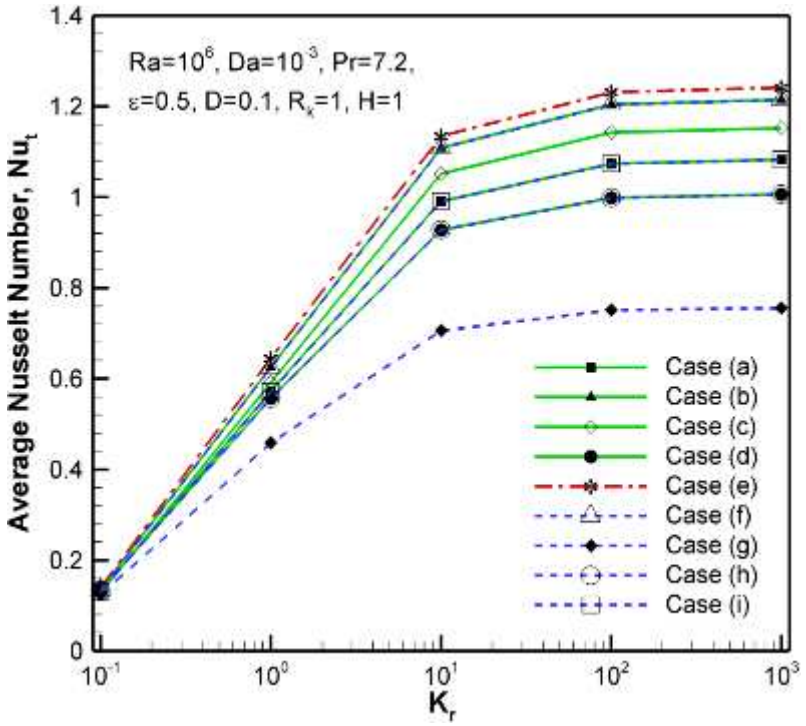


**Fig. 12.** Variation of $Nu_t$ with $K_r$ for different thermally active locations.

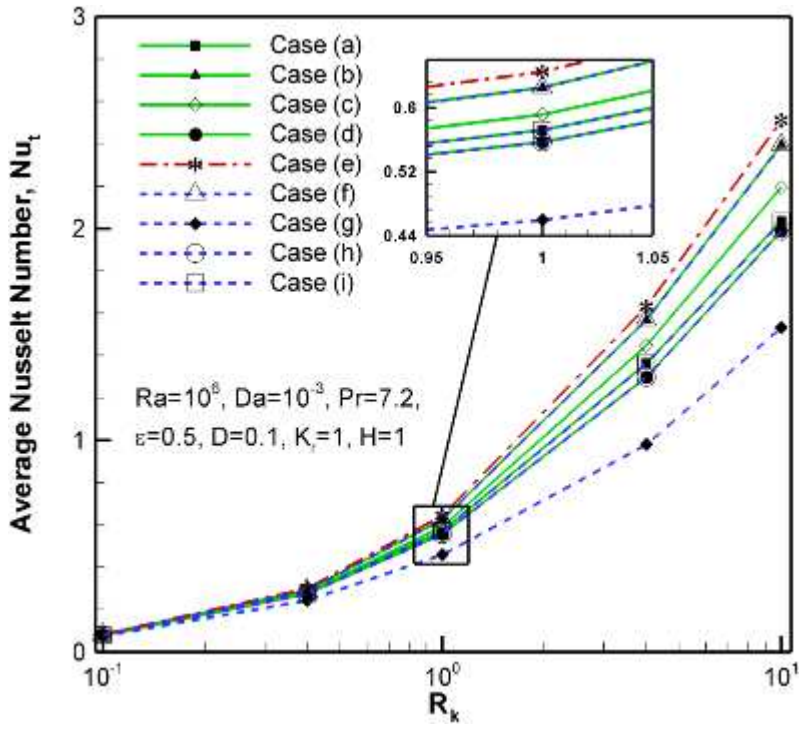


**Fig. 13.** Variation of $Nu_t$ with $R_k$ for different thermally active locations.

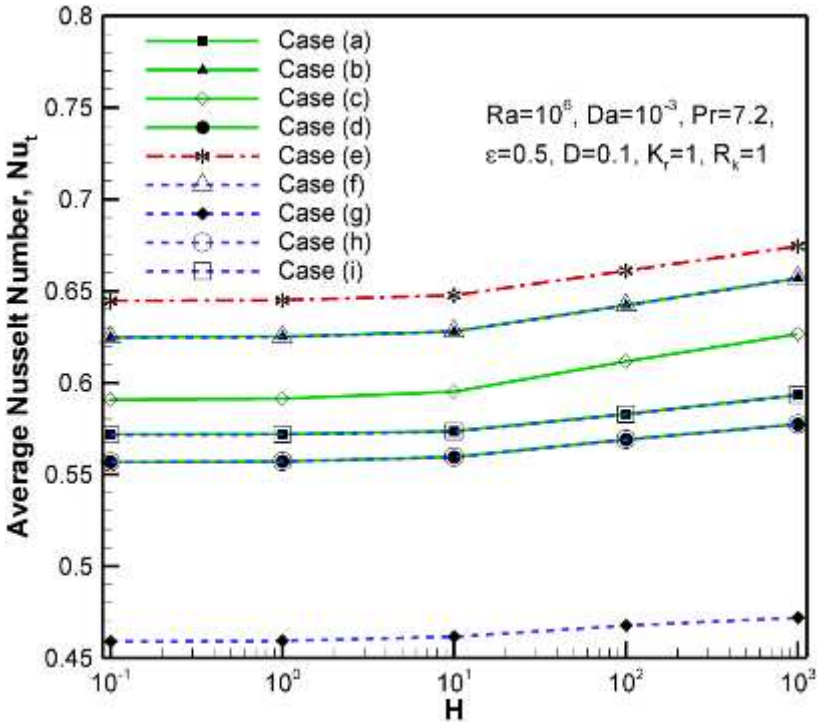


**Fig. 14.** Variation of $Nu_t$ with $H$ for different thermally active locations.

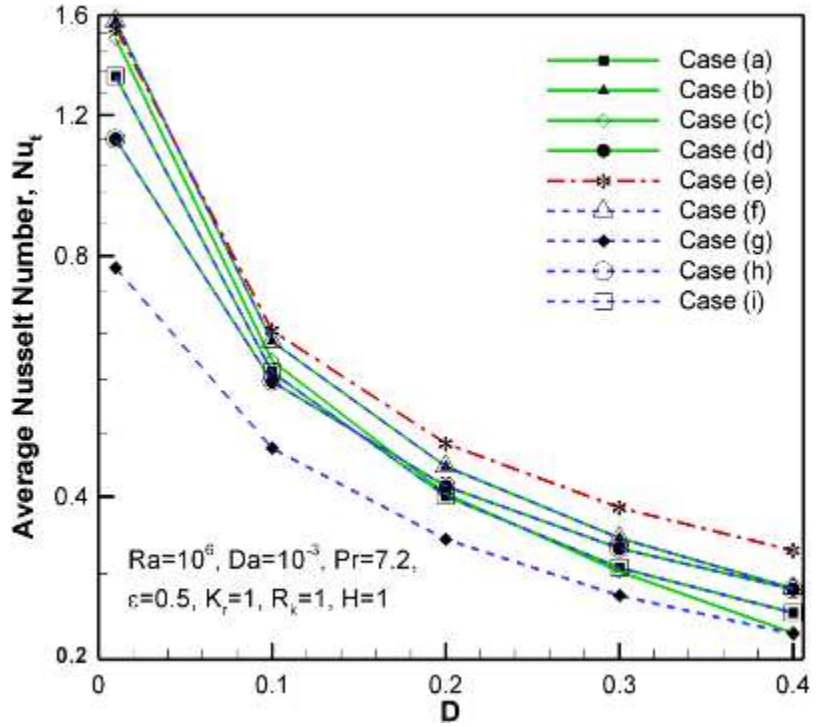


**Fig. 15.** Variation of $Nu_t$ with $D$ for different thermally active locations.

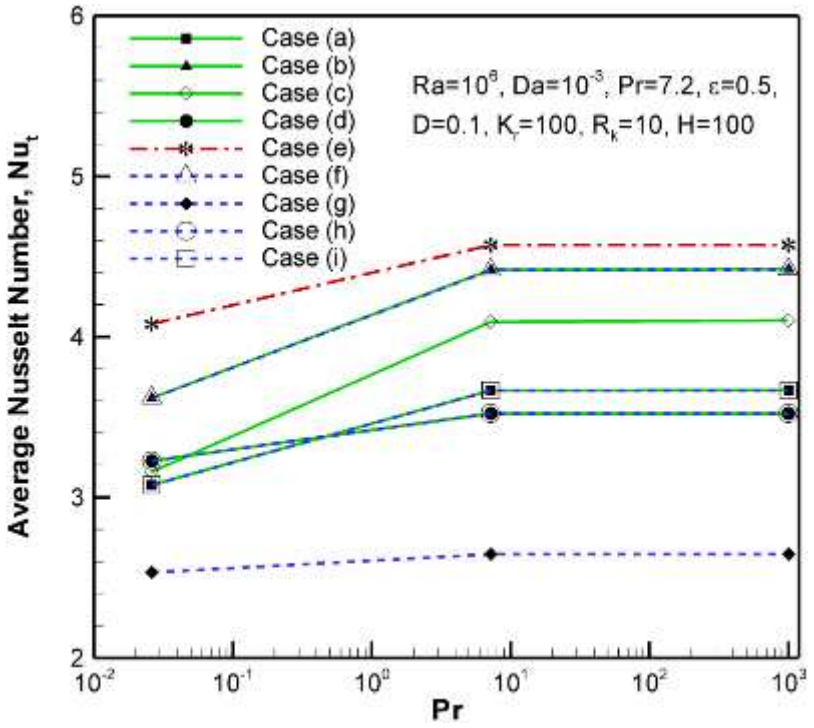


**Fig. 16.** Variation of $Nu_t$ with $Pr$ for different thermally active locations.

## 5. Conclusion

The flow and heat transfer in a porous cavity filled with a porous medium is studied by the two equation heat transfer model; one for the fluid inside the pores and one for the porous matrix. The heat transfer bifurcation at the solid walls and the porous medium is modelled using the temperature continuity, energy balance and the effective thermal conductivity, and the effect of local thermal non-equilibrium is studied. The governing equations are transformed into a non-dimensional form, and solved by the finite element method. The results are reported in the form of streamlines and isotherms, as well as the average Nusselt number of each phase and the overall average Nusselt number. The key results of the present study can be summarized as follows:

1- The location of the cold and hot elements shows important effects on the flow and heat transfer in the cavity. However, the parameters such as the Rayleigh number, Darcy

number, the the porous-fluid thermal conductivity ratio parameter, and the wall to fluid thermal conductivity ratio parameter can affect the trend of the results for the average Nusselt number in the fluid phase and porous matrix phase.

2- The small values of Prandtl number (Pr<1) can change the overall trend of the behaviour of the location of elements for the total average Nusselt number (total heat transfer rate). Indeed, the low Prandtl number boosts the thermal diffusion mechanism compared to the convective mechanism, and hence, it can alter the trend of the behavior of the element locations. Similarly, Rayleigh number can also slightly change the trend of the results by change in the order of diffusion and convection mechanisms.

3- The change in the order of the wall to fluid thermal conductivity ratio parameter ($R_k$) from 10 to 0.1 can significantly reduce the overall heat transfer by inducing insulation areas that act as thermal barriers next to the active walls.

4- Interestingly, the results of the LTNE model indicate that there is an optimum value of the porous-fluid interface convection parameter (H) about H≈10.

5. Considering the thermal conductivity of the thick walls comparable with the thermal conductivity of the fluid and the matrix of the porous medium ($R_k \approx K_r \approx 1$), the increase of thickness of the solid walls decreases the overall heat transfer due to the reduction of the convective heat transfer mechanism

6- The increase of the Prandtl number up to the order of 10 increased the overall heat transfer. However, the further increase of this parameter does not show any significant effect on the overall heat transfer in the cavity.

**References**


[1] C.-B. Huang and X.-J. Zhu, "Heat dissipating device with metal foam," U.S. Patent Application Patent 11/166,662, 2005.

[2] R. Wirtz, "Porous media heat sink apparatus," U.S. Patent Application Patent 09/734,526, 2000.

[3] G. A. DiBattista, T. L. Mace, J. P. Wingo, and G. Mao, "Thermally conductive porous media," U.S. Patent Application Patent 14/344,212, 2012.
[4] D. R. Sabatino, S. F. Kaslusky, H. M. Reeve, L. J. Spadaccini, L. Chiappetta, H. Huang, *et al.*, "Metal foam heat exchanger," U.S. Patent 8,127,829, 2012.
[5] T. Basak, S. Roy, T. Paul, and I. Pop, "Natural convection in a square cavity filled with a porous medium: effects of various thermal boundary conditions," *International Journal of Heat and Mass Transfer,* vol. 49, pp. 1430-1441, 2006.
[6] M. Sathiyamoorthy, T. Basak, S. Roy, and I. Pop, "Steady natural convection flow in a square cavity filled with a porous medium for linearly heated side wall (s)," *International Journal of Heat and Mass Transfer,* vol. 50, pp. 1892-1901, 2007.
[7] M. A. Sheremet and I. Pop, "Natural convection in a square porous cavity with sinusoidal temperature distributions on both side walls filled with a nanofluid: Buongiorno's mathematical model," *Transport in Porous Media,* vol. 105, pp. 411-429, 2014.
[8] Y. Varol, H. F. Oztop, and I. Pop, "Numerical analysis of natural convection in an inclined trapezoidal enclosure filled with a porous medium," *International Journal of Thermal Sciences,* vol. 47, pp. 1316-1331, 2008.
[9] A. J. Chamkha and M. A. Ismael, "Natural convection in differentially heated partially porous layered cavities filled with a nanofluid," *Numerical Heat Transfer, Part A: Applications,* vol. 65, pp. 1089-1113, 2014.
[10] M. A. Sheremet, T. Grosan, and I. Pop, "Free convection in a square cavity filled with a porous medium saturated by nanofluid using Tiwari and Das' nanofluid model," *Transport in Porous Media,* vol. 106, pp. 595-610, 2015.
[11] N. H. Saeid and I. Pop, "Natural convection from a discrete heater in a square cavity filled with a porous medium," *Journal of Porous Media,* vol. 8, 2005.
[12] N. H. Saeid and I. Pop, "Transient free convection in a square cavity filled with a porous medium," *International journal of heat and mass transfer,* vol. 47, pp. 1917-1924, 2004.
[13] M. A. Sheremet, I. Pop, and A. Shenoy, "Unsteady free convection in a porous open wavy cavity filled with a nanofluid using Buongiorno's mathematical model," *International Communications in Heat and Mass Transfer,* vol. 67, pp. 66-72, 2015.
[14] M. A. Sheremet, I. Pop, and N. Bachok, "Effect of thermal dispersion on transient natural convection in a wavy-walled porous cavity filled with a nanofluid: Tiwari and Das' nanofluid model," *International Journal of Heat and Mass Transfer,* vol. 92, pp. 1053-1060, 2016.
[15] A. Baytaş, A. Liaqat, T. Groşan, and I. Pop, "Conjugate natural convection in a square porous cavity," *Heat and Mass transfer,* vol. 37, pp. 467-473, 2001.
[16] N. H. Saeid, "Conjugate natural convection in a porous enclosure: effect of conduction in one of the vertical walls," *International Journal of Thermal Sciences,* vol. 46, pp. 531-539, 2007.
[17] N. H. Saeid, "Conjugate natural convection in a vertical porous layer sandwiched by finite thickness walls," *International communications in heat and mass transfer,* vol. 34, pp. 210-216, 2007.
[18] A. Alhashash, H. Saleh, and I. Hashim, "Conjugate natural convection in a porous enclosure sandwiched by finite walls under the influence of non-uniform heat generation and radiation," *Transport in porous media,* vol. 99, pp. 453-465, 2013.
[19] M. A. Sheremet and I. Pop, "Conjugate natural convection in a square porous cavity filled by a nanofluid using Buongiorno's mathematical model," *International Journal of Heat and Mass Transfer,* vol. 79, pp. 137-145, 2014.

[20] H. Saleh, N. Saeid, I. Hashim, and Z. Mustafa, "Effect of conduction in bottom wall on Darcy–Bénard convection in a porous enclosure," *Transport in porous media,* vol. 88, pp. 357-368, 2011.
[21] M. A. Ismael, T. Armaghani, and A. J. Chamkha, "Conjugate heat transfer and entropy generation in a cavity filled with a nanofluid-saturated porous media and heated by a triangular solid," *Journal of the Taiwan Institute of Chemical Engineers,* vol. 59, pp. 138-151, 2016.
[22] A. C. Baytas and I. Pop, "Free convection in a square porous cavity using a thermal nonequilibrium model," *International Journal of Thermal Sciences,* vol. 41, pp. 861-870, 2002.
[23] A. Baytas, "Thermal non-equilibrium free convection in a cavity filled with a non-Darcy porous medium," in *Emerging Technologies and Techniques in Porous Media*, ed: Springer, 2004, pp. 247-258.
[24] F. Wu, W. Zhou, and X. Ma, "Natural convection in a porous rectangular enclosure with sinusoidal temperature distributions on both side walls using a thermal non-equilibrium model," *International Journal of Heat and Mass Transfer,* vol. 85, pp. 756-771, 2015.
[25] F. Wu, W. Zhou, G. Wang, X. Ma, and Y. Wang, "Numerical Simulation of Natural Convection in a Porous Cavity with Linearly Temperature Distributions Under the Local Thermal Nonequilibrium Condition," *Numerical Heat Transfer, Part A: Applications,* vol. 68, pp. 1394-1415, 2015.
[26] F. Wu, G. Wang, and W. Zhou, "Aspect ratio effect on natural convection in a square enclosure with a sinusoidal active thermal wall using a thermal non-equilibrium model," *Numerical Heat Transfer, Part A: Applications,* vol. 70, pp. 310-329, 2016.
[27] A. Tahmasebi, M. Mahdavi, M. Ghalambaz "Local thermal nonequilibrium conjugate natural convection heat transfer of nanof luids in a cavity partially filled with porous media using Buongiorno's model", *Numerical Heat Transfer, Part A: Applications*, 2018.
[28] H. Zargartalebi, M. Ghalambaz, A. Noghrehabadi, and A. J. Chamkha, "Natural convection of a nanofluid in an enclosure with an inclined local thermal non-equilibrium porous fin considering Buongiorno's model," *Numerical Heat Transfer, Part A: Applications,* vol. 70, pp. 432-445, 2016.
[29] K. Yang and K. Vafai, "Analysis of temperature gradient bifurcation in porous media–an exact solution," *International Journal of Heat and Mass Transfer,* vol. 53, pp. 4316-4325, 2010.
[30] K. Yang and K. Vafai, "Restrictions on the validity of the thermal conditions at the porous-fluid interface—an exact solution," *Journal of Heat Transfer,* vol. 133, p. 112601, 2011.
[31] K. Yang and K. Vafai, "Analysis of heat flux bifurcation inside porous media incorporating inertial and dispersion effects–an exact solution," *International Journal of Heat and Mass Transfer,* vol. 54, pp. 5286-5297, 2011.
[32] D. A. Nield, "A note on local thermal non-equilibrium in porous media near boundaries and interfaces," *Transport in porous media,* vol. 95(3), pp. 581-584, 2012.
[33] K. Vafai and K. Yang, "A note on local thermal non-equilibrium in porous media and heat flux bifurcation phenomenon in porous media," *Transport in porous media,* vol. 96, pp. 169-172, 2013.
[34] N. H. Saeid, "Conjugate natural convection in a porous enclosure sandwiched by finite walls under thermal nonequilibrium conditions," *Journal of Porous Media,* vol. 11, 2008.

[35] T. Basak, S. Roy, A. Singh, and A. Balakrishnan, "Natural convection flows in porous trapezoidal enclosures with various inclination angles," *International Journal of Heat and Mass Transfer,* vol. 52, pp. 4612-4623, 2009.
[36] K. Vafai and C. Tien, "Boundary and inertia effects on flow and heat transfer in porous media," *International Journal of Heat and Mass Transfer,* vol. 24, pp. 195-203, 1981.
[37] K. Vafai and S. Kim, "On the limitations of the Brinkman-Forchheimer-extended Darcy equation," *International Journal of Heat and Fluid Flow,* vol. 16, pp. 11-15, 1995.
[38] D. A. Nield and A. Bejan, *Convection in porous media*, fourth ed.: Springer Science & Business Media, 2013.
[39] D. Nield, "Estimation of the stagnant thermal conductivity of saturated porous media," *International journal of heat and mass transfer,* vol. 34, pp. 1575-1576, 1991.
[40] S. Rao, "The finite element method in engineering. Butter-worth," ed: Heinemann publications, Amsterdam, Boston, Heidelberg, London, New York, Oxford Paris, San Diego, San Francisco, Singapore, Sydney, Tokyo, 2005.
[41] P. Wriggers, *Nonlinear finite element methods*: Springer Science & Business Media, 2008.
[42] P. R. Amestoy, I. S. Duff, and J.-Y. L'Excellent, "Multifrontal parallel distributed symmetric and unsymmetric solvers," *Computer methods in applied mechanics and engineering,* vol. 184, pp. 501-520, 2000.
[43] G. Lauriat and V. Prasad, "Non-Darcian effects on natural convection in a vertical porous enclosure," *International Journal of Heat and Mass Transfer,* vol. 32, pp. 2135-2148, 1989.